Biomedicine & Pharmacotherapy 168 (2023) 115789

Contents lists available at ScienceDirect

Biomedicine & Pharmacotherapy

journal homepage: www.elsevier.com/locate/biopha

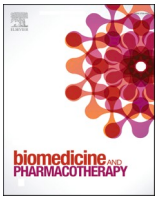

Antitumor activity of bengamide ii in a panel of human and murine tumor cell lines: *In vitro* and *in vivo* determination of effectiveness against lung cancer

Alba Ortigosa-Palomo [a,b,c], Cristina Porras-Alcalá [d], Francisco Quiñonero [a,c], Federico Moya-Utrera [d], Raúl Ortiz [a,b,c,*], Juan M. López-Romero [d], Consolación Melguizo [a,b,c], Francisco Sarabia [d,1], Jose Prados [a,b,c,1]

[a] Institute of Biopathology and Regenerative Medicine (IBIMER), Center of Biomedical Research (CIBM), University of Granada, 18100 Granada, Spain
[b] Department of Anatomy and Embryology, Faculty of Medicine, University of Granada, 18071 Granada, Spain
[c] Instituto de Investigación Biosanitaria ibs.GRANADA, 18012 Granada, Spain
[d] Department of Organic Chemistry, Faculty of Sciences, University of Malaga, 29071 Málaga, Spain

ARTICLE INFO

Keywords:
Bengamide II
Lung cancer
Antitumor
in vitro
in vivo

ABSTRACT

Lung cancer is the most commonly diagnosed cancer and the one that causes the most deaths worldwide, so there is a need for therapies that improve survival rates. Products derived from marine organisms are a source of novel and potent antitumor compounds, but they present the great obstacle of their obtaining from the natural environment and the problems associated with the synthesis and biological effects of chemical analogues. In this work, a Bengamide analogue (Bengamide II) was chemically synthesized and *in vitro* and *in vivo* studies were performed to determine its antitumor activity and mechanisms of action. It was shown to have potent antiproliferative activity in lung cancer lines in 2D and 3D models. In addition, Bengamide II-treated cells showed G2/M and G0/G1 cell cycle arrest, together with a decrease in the proliferation marker Ki67. As for the mechanism of action, the treatment was associated with increased LC3-II expression and production of acidic vesicles signaling autophagy. In addition, Bengamide II treatment was associated with caspase-3 activation and DNA fragmentation related to apoptosis. Furthermore, a reduction of VEGFA expression, related to angiogenesis, was also observed. *In vivo* studies showed that Bengamide II markedly reduced tumor volume and metastases increasing survival. Additionally, it revealed no systemic toxicity in *in vivo* models at the therapeutic doses used, which is essential for its future clinical use. Taken together, the chemically synthesized bengamide analogue Bengamide II, is a promising drug for lung cancer treatment showing relevant antitumor activity and significant safety.

1. Introduction

Bengamides comprise a large number of members of a family of naturally occurring compounds of marine origin. The discovery of the first members of bengamides, A (**1**) and B (**2**), was in 1986 by Crews and Quinoa from an undescribed specimen of a sponge belonging to the *Jaspidae* family in the Fiji Islands [1]. Following this first discovery, other members of the bengamides (bengamides C-Q) were isolated from sponges in other parts of the world [2]. Interestingly, in 2012, Johnson et al. reported the existence of bengamides, in particular bengamides E (**3**), F (**4**), E′ (**5**) and F′ (**6**) in a gram negative terrestrial bacterium, *Myxococcus virescens* [3]. These natural compounds displayed impressive biological activities, including antitumor, anthelmintic and antibiotic activities, what encouraged an intense research activity towards the design, synthesis, and biological evaluation of analogues in the last years [4,5].

The robust and outstanding antitumor effects of some of the natural bengamides and analogues have attracted the attention of several

* Corresponding author at: Institute of Biopathology and Regenerative Medicine (IBIMER), Center of Biomedical Research (CIBM), University of Granada, 18100 Granada, Spain.
E-mail address: roquesa@ugr.es (R. Ortiz).
[1] Co-Senior authors: equal contribution

https://doi.org/10.1016/j.biopha.2023.115789
Received 14 September 2023; Received in revised form 16 October 2023; Accepted 26 October 2023
Available online 2 November 2023

research groups, and some of the mechanisms by which they exert this antitumor effect have been investigated and are now known. *In vitro* studies have documented the antiproliferative effects of bengamide analogues, while *in vivo* assays have been conducted to evaluate their efficacy against breast cancer and melanoma mouse model. Additionally, a clinical trial developed by Novartis was undertaken; however, it was discontinued due to cardiac toxicity [2]. Recently, bengamide analogues have shown no toxic effects in blood cells and cells of the immune system (macrophages and white blood cells) [6].

The molecular target of bengamides was elucidated by proteomics-based approach, showing that bengamides inhibited the methionine aminopeptidases, MetAp1 and MetAp2, and revealing that cells treated with bengamide had an increase in N-terminal methionine residues of 20% [7]. This action mechanism was supported by the crystalization of the enzyme-bengamide complex and subsequent X-ray analysis [7,8], together with enzymatic assays that showed an inhibitory effect of bengamides against MetAp1 and MetAp2 activity [9,10]. As a consequence of MetAps inhibition, bengamide hampered N-myristoylation of proto-oncogene *c-Src*, which play a pivotal role in cell cycle progression, altered its subcellular localization and significantly decreased its tyrosine kinase activity, producing a delay in cell cycle progression through G2/M phase [6,10]. In addition, bengamides exert immunomodulatory effect through targeting nuclear factor kB (NF-kB) pathway implicated in development and metastasis in several cancers [3]. Furthermore, MetAp2 enzyme inhibition has gained interest as a cancer treatment strategy as it is a well-known target of anti-angiogenic and tumor growth suppressor drugs such as ovalicin [11] and fumagillin [12]. Additionally, Wenzel et al. suggested that bengamide could be recognized by P-glycoprotein efflux pump, an important detoxifying protein located in cell membrane [13].

Among all the bengamide analogues reported so far, the ring-opened derivatives, developed by Tai et al. exhibited very potent activities (Scheme 1) and improved solubilities in water with respect to the natural counterparts. Particularly striking was compound **8**, which was found to be the most potent analogue of the series (IC_{50} = 4 nM against MDA-MB-435), displaying an excellent solubility in water (7.57 mg/mL) [14]. Given the promising antitumor properties showed by this bengamide analogue, we decided to prepare it, according to our synthetic strategy established for the bengamides, and to further investigate its antitumor activities.

On the other hand, lung cancer, the second most frequently diagnosed cancer (11.4% of all cancers) and the leading cause of cancer-related death worldwide (18% of all cancer deaths) in 2020 [15], needs new therapeutic strategies to improve the survival rate of patients. In fact, non-small cell lung cancer (NSCLC), the most common type of lung cancer (85% of lung cancer), has progressively increased its incidence and mortality in recent years [16] despite advances in the application of predictive and diagnostic biomarkers and healthier lifestyles [17]. Surgical resection, chemotherapy, radiation, immunotherapy, targeted molecular therapy, and/or their combination are the current treatment for NSCLC [18]. Surgical resection in early stages (stage I) offers a favorable prognosis with a 5-year survival rate of 70–90%. However, advanced-stage NSCLC (more than 60% of diagnoses are stage III or IV) is unresectable showing an overall 5-year survival rate of about 15% despite multiple drugs available for treatment [19]. The development of drug resistance is the main cause of treatment failure and poor prognosis. In fact, drug resistance appears not only against conventional chemotherapy treatments, but also against targeted molecular therapies [20]. Therefore, it is mandatory to develop new therapeutic tools to improve the prognosis of patients with NSCLC.

The main objective of this study was to analyze the antitumor effect of a new bengamide (Bengamide II) first in a panel of tumor cell lines and later, in view of the obtained results, specifically in NSCLC cells. Although future trials will be necessary, these results suggest that Bengamide II may be a promising new molecule for the treatment of this type of tumor.

2. Materials and methods

2.1. General techniques

All reactions were carried out under an argon atmosphere with dry, freshly distilled solvents under anhydrous conditions, unless using aqueous reagents or otherwise noted. All solvents used in reactions were dried and distilled using standard procedures. Tetrahydrofuran (THF) was distilled from sodium benzophenone, and methylene chloride (CH_2Cl_2) from calcium hydride. Yields refer to chromatographically and spectroscopically (^{1}H NMR) homogeneous materials, unless otherwise stated. All solutions used in workup procedures were saturated unless otherwise noted. All reagents were purchased at highest commercial

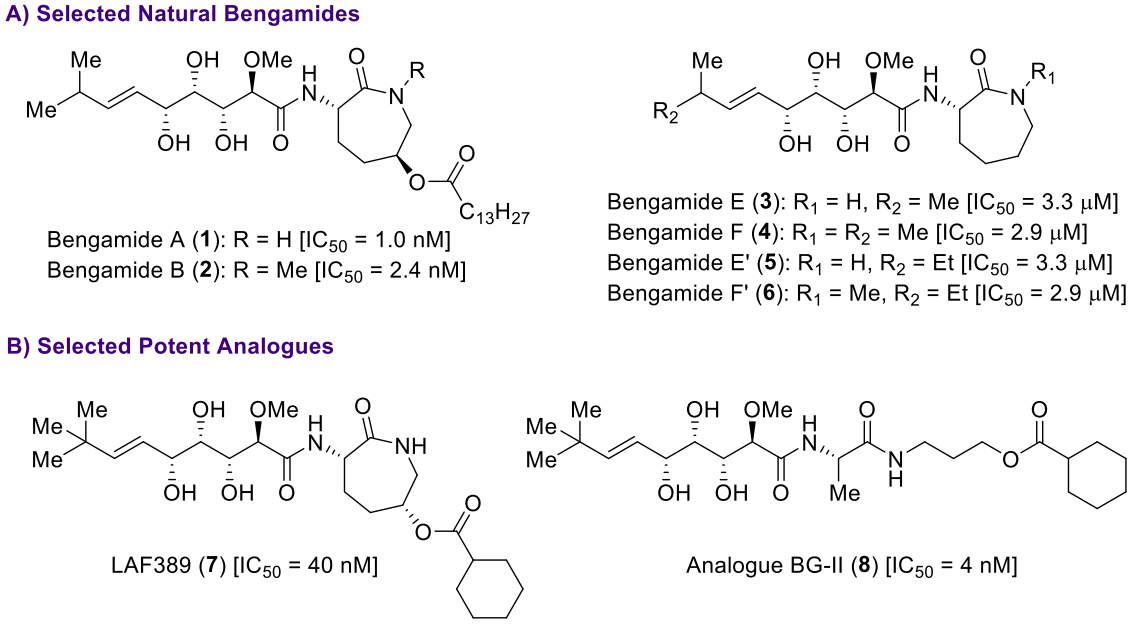

Scheme 1. Natural Bengamides and Bengamide analogues. (A) Molecular structures of representative natural bengamides; (B) Representative bengamide analogues and their cytotoxicities against MDA-MB-435 human breast cancer cells.

quality and used without further purification unless otherwise stated. All reactions were monitored by thin-layer chromatography (TLC) using 0.25 mm silica gel plates (60 F-254) using UV light (254 nm) as visualizing agent and acidic ceric ammonium molybdate/ phosphomolybdic acid or potassium permanganate solutions and heat as developing agents. Flash column chromatography (FCC) was performed using silica gel (60 Å, particle size 230–400 mesh) under air pressure. All solvents used for chromatographic purifications were distilled prior to use. ^{1}H and ^{13}C NMR spectra were recorded on a Bruker DPX-400 MHz instrument (Fällanden, Switzerland) and calibrated using residual undeuterated solvent as an internal reference. Chemical shifts are reported in ppm with the resonance resulting from incomplete deuteration of the solvent as the internal standard ($^{13}CDCl_3$: 7.26 ppm, s and 77.0 ppm, t; $^{13}CD_3OD$: 4.87 ppm, s, 3.31 ppm, quin and 49.1 ppm, sep; $^{13}C_2D_6OS$: 2.49 ppm, quin and 39.52 ppm, sep). Data are reported as follows: chemical shift δ/ppm (multiplicity, coupling constants J (Hz) and integration (^{1}H only)). The following abbreviations were used to explain the multiplicities: s = singlet; d = doublet; t = triplet; q = quartet; quin = quintet; b = broad; m = multiplet or combination thereof. ^{13}C signals are singles, unless otherwise stated. High-resolution mass spectrometry (HRMS) was performed on a Thermo Fisher Scientific H-ESI and APCI mass spectrometer (Waltham (MA), USA) in positive mode and using an ion trap (Orbitrap) as the mass analyzer type. HRMS signals are reported to four decimal places and are within ± 5 ppm of theoretical values.

2.2. Synthesis of the Bengamide Analogue 8

Alkene **11**. Olefin **9** (85 mg, 0.37 mmol, 1.0 equiv) and Hoveyda-Grubbs 2nd generation catalyst (38 mg, 0.06 mmol, 0.15 equiv) were dissolved in degassed CH_2Cl_2 (8.0 mL). Then 3,3-dimethylbut-1-ene (10) (2.0 mL) was added dropwise at room temperature. The resulting mixture reaction was heated at 40ºC for 12 h. After this time, the solvent was removed *in vacuo* and the resulting crude product was purified by flash column chromatography (Silica gel, 100% hexanes → 40% EtOAc in hexanes) to obtain **11** (96 mg, 90%) as a brown solid: R_f: 0.72 (silica gel, 40% EtOAc in hexanes); ^{1}H NMR (400 MHz, $CDCl_3$): δ 5.87 (d, J = 15.6 Hz, 1 H), 5.33 (dd, J = 15.6, 8.2 Hz, 1 H), 4.56 (d, J = 6.8 Hz, 2 H), 4.40 (t, J = 8.4 Hz, 1 H), 3.45 (s, 3 H), 3.19 (dt, J = 7.7, 4.0 Hz, 2 H), 1.46 (s, 3 H), 1.44 (s, 3 H), 1.03 (s, 9 H).

Carboxylic acid **12**. BAIB (100 mg, 0.30 mmol, 3.0 equiv) was added to a stirred solution of diol **11** (30 mg, 0.10 mmol, 1.0 equiv) in a 1:1 mixture of acetonitrile: water (4.0 mL). Then, 2,2,6,6-tetramethyl-1-piperidinyloxy (TEMPO) (4.6 mg, 0.03 mmol, 0.3 equiv) was added and the resulting reaction mixture was stirred for 12 h at room temperature. After this time, the reaction was quenched by addition of a saturated aqueous $Na_2S_2O_3$ solution and the aqueous layer was extracted with AcOEt. The combined organic extracts were washed with brine, dried over anhydrous $MgSO_4$, filtered and concentrated under reduced pressure to yield carboxylic acid **12** as a light yellow oil, which was used in the next step without any further purification.

Compound **14**. To a solution of crude acid 12 (~ 0.30 mmol, 1.0 equiv) in DMF (3 mL) were added DIPEA (0.18 mL, 0.99 mmol, 3.3 equiv) and amino acid derivative **13** (133 mg, 0.36 mmol, 1.2 equiv). When the solution was homogeneous, BOP (159 mg, 0.36 mmol, 1.2 equiv) was added in one portion, and the reaction mixture was stirred for 12 h at room temperature. After this time, Et_2O was added, and the organic phase was washed with a saturated aqueous NH_4Cl solution. The organic layer was dried over anhydrous $MgSO_4$, filtered and solvents were removed in vacuo. The resulting crude product was purified by flash column chromatography (Silica gel, 60% EtOAc in hexanes) to obtain compound **14** (133 mg, 82% over 2 steps from 11) as a white solid. R_f: 0.60 (silica gel, 100% EtOAc); ^{1}H NMR (400 MHz, $CDCl_3$) δ 6.90 (d, J = 7.2 Hz, 1 H), 6.76 – 6.71 (m, ^{1}H), 5.89 – 5.82 (m, 1 H), 5.41 (dd, J = 15.6, 8.3 Hz, 1 H), 4.54 – 4.43 (m, 1 H), 4.39 – 4.29 (m, 2 H), 4.11 (t, J = 6.0 Hz, 2 H), 3.92 (dd, J = 8.4, 3.9 Hz, 2 H), 3.72 (t, J = 5.6 Hz, 2 H), 3.46 (s, J = 6.6 Hz, 3 H), 3.32 – 3.22 (m, 2 H), 2.37 – 2.24 (m, 3 H), 1.92 – 1.72 (m, 8 H), 1.43 (d, J = 1.4 Hz, 6 H), 1.04 (s, 9 H). ^{13}C NMR (101 MHz, $CDCl_3$) δ 171.58, 170.60, 148.47, 132.42, 130.08, 128.29, 121.68, 109.00, 81.76, 79.33, 79.15, 71.25, 61.32, 59.13, 48.55, 43.22, 36.20, 33.25, 29.71, 29.27, 29.05, 28.66, 27.27, 26.93, 25.72, 25.42, 22.70, 17.91, 14.13; HRMS (H-ESI) m/z: $[M + H]^+$ calculated for $C_{28}H_{49}N_2O_8$ 541.3489; found 541.3485.

Bengamide analogue **8**. HCl (1 M, 15 mL) was added to a stirred solution of compound **14** (133 mg, 0.25 mmol, 1.0 equiv) in THF (20 mL). The resulting reaction mixture was vigorously stirred for 4 h at room temperature. After this time, the reaction mixture was diluted with EtOAc and the excess of HCl was quenched by addition of a saturated aqueous $NaHCO_3$ solution. The aqueous layer was extracted with AcOEt, the organic layer washed with brine, dried over anhydrous $MgSO_4$, filtered and concentrated under reduced pressure. The resulting crude product was purified by flash column chromatography (Silica gel, 60% EtOAc in hexanes → 20% MeOH in CH_2Cl_2) to obtain bengamide analogue 8 (103.8 mg, 83%) as a colourless oil: R_f: 0.1 (silica gel, 10% MeOH in DCM); ^{1}H NMR (400 MHz, $CDCl_3$): δ 7.13 (s, 1 H), 6.79 (s, 1 H), 5.84 (d, J = 15.7 Hz, 1 H), 5.49 (dd, J = 15.6, 6.4 Hz, 1 H), 4.55 – 4.40 (m, 2 H), 4.27 – 4.18 (m, 1 H), 4.10 (t, J = 6.5 Hz, 2 H), 4.00 (s, 1 H), 3.83 (d, J = 4.2 Hz, 1 H), 3.69 (s, 1 H), 3.50 (s, 3 H), 3.40 – 3.26 (m, 2 H), 3.18 (dt, J = 13.5, 6.2 Hz, 1 H), 2.35 – 2.24 (m, 2 H), 1.95 – 1.70 (m, 8 H), 1.45 (d, J = 7.2 Hz, 3 H), 1.25 (s, 4 H), 1.03 (s, J = 0.9 Hz, 9 H); HRMS (H-ESI) m/z: $[M + H]^+$ calculated for $C_{25}H_{45}N_2O_8$ 501.3176; found 501.3158.

2.3. Cell culture

Human lung (A549, NCIH460, NCIH520), breast (MCF7, SKBR3), pancreas (PANC1), central nervous system (SK-N-SH, A172, SF268, LN229), colon (T84) and liver (HepG2) cancer cell lines, murine breast (E0771), pancreas (PANC2), lung (LL2) and colon (MC38) cancer cell lines and colon (CCD18Co) non-tumor cell line were grown in Dulbecco's Modified Eagle's Medium (DMEM)-high glucose (Sigma-Aldrich). H69 lung cancer cell line was grown in RPMI 1640 medium (Sigma-Aldrich) and breast cancer cell line MDA-MB-231 in Dulbecco's Modified Eagle's Medium/Nutrient Mixture F-12 Ham (Sigma-Aldrich). Culture mediums were supplemented with 10% of Fetal Bovine Serum (FBS) (Gibco) and 1% of Penicillin/Streptomycin (Sigma-Aldrich). Furthermore, MCF10A breast non-tumor cell line was grown in Dulbecco's Modified Eagle's Medium/Nutrient Mixture F-12 Ham (Sigma-Aldrich) supplemented with 5% horse serum (HS) (Sigma-Aldrich), 0.02 μg/mL epithelial growth factor (EGF) (Sigma-Aldrich), 0.5 μg/mL hydrocortisone (Sigma-Aldrich), 100 ng/mL cholera toxin (Sigma-Aldrich) and 0.01 μg/mL insulin-transferrin-selenium (ITS) (Thermo Fisher Scientific). Cells were maintained at 37 °C and 5% CO_2 humidified atmosphere. Scheme S1 shows a summary of the cell types used and most relevant information about Material and Methods.

2.4. Proliferation assay

Cell lines were seeded in 48 well-plates at a density between 2.5×10^3 and 5×10^4 cells/well in order to calculate the half maximal inhibitory concentration (IC_{50}) of Bengamide II (BII) in each cell line. This study focus on lung cancer, so human non-small cell lung cancer A549, NCIH460 and NCIH520 cell lines, human small cell lung cancer H69 cell line and murine lung cancer LL/2 cell line were the most widely studied. Cell lines were seeded in 48-well plates at a density of 4×10^3 cells/well for LL/2, 5×10^3 cells/well for A549, 6×10^3 cells/well for NCIH460, and 10^4 cells/well for H69. NCIH520 were seeded in 96-well plates at a density of 1.5×10^4 cells/well. After 24 h cells were incubated with increasing concentration (0.01–10 μM) of the drug (Bengamide II) for 72 h. Thus, adherent cell lines were fixed with cold trichloroacetic acid (TCA) (Sigma-Aldrich) 10% for 20 min at 4ºC and stained for 20 min at room temperature with Sulforhodamine B (SRB) (Sigma-Aldrich) (0.08%) diluted in 1% acetic acid glacial (PanReac

AppliChem). The dye was solubilized using Trizma® (10 mM, pH 10.5) (Sigma-Aldrich). Finally, the optical density (OD) was measured at 492 nm using 800™ TS Absorbance Reader (BioTek). Viability assay of H69 cell line was performed using Cell Counting Kit-8 (CCK-8) (Dojindo Laboratories, Kumamoto, Japan) 10% in RPMI, incubating cells for 3 h at 37 °C and the absorbance at 450 nm was determined. Cell viability (%) was calculated as follows:

$$\%Proliferation = \frac{OD\ \ sample - blank}{OD\ \ negative\ \ control - blank}\ \ x100$$

2.5. Clonogenic assay

A549, NCIH460 and LL2 cell lines were pretreated with IC_{50} of Bengamide II (0.4, 0.15 and 4 μM respectively). After 72 h, surviving pretreated cells and non-treated cells were seeded at different densities for A549 (10^2 cells/well), NCIH460 (2×10^2 cells/well) and LL2 (10^2 cells/well) in 12-well plates. A549, NCIH460 and LL2 non-treated cells were treated with IC_{10} (0.05, 0.05 and 1 μM respectively) and IC_{25} (0.1, 0.1 and 3 μM respectively) of Bengamide II. The reduction of colony number was assessed after 14 days (A549 and NCIH460) or 6 days (LL2) of incubation at 37 °C in fully humidified atmosphere and 5% CO_2. Colonies were fixed with cold TCA (Sigma-Aldrich) 10% for 20 min at 4ºC and stained for 20 min at room temperature with SRB (Sigma-Aldrich) (0.08%) diluted in 1% acetic acid glacial (PanReac AppliChem), photos of the 12-well plate were taken, and colonies were counted through ImageJ software.

2.6. Multicellular tumor spheroid (MTS) assay

Multicellular tumor spheroids of different lung cancer cell lines were generated following our previously described protocol [21]. Briefly, a 96-well plate was coated with 50 μl of 1% agarose (w/v) to avoid cell adhesion and dried at room temperature. Therefore, A549 (2×10^3 cells/well), LL/2 and NCIH460 (5×10^2 cells/well) were seeded. The plates were centrifuged at 2230 rpm for 10 min to facilitate cellular aggregation and single spheroid formation per well. The plates were maintained at 37 °C and 5% CO_2 humidified atmosphere for 72 h to allow them to take the three-dimensional spheroid form. After that, medium was changed and MTS were treated with a concentration equivalent to IC_{50} (IC50), 2 times IC_{50} (2IC50) and 4 times IC_{50} (4IC50) doses of Bengamide II (Day 0). Untreated MTS were used as negative control. New medium change and re-addition of Bengamide II were made after three days (Day 3). Three days later (Day 6), a new medium change was performed, and MTS were maintained three more days without any treatment. To monitor the MTS growth, photos were taken every three days until the end of experiment (Day 9) using a photographic inverted Microscope (Olympus, CKX41). Spheroid volume was calculated mathematically with the longest diameter (LD) and the shortest diameter (SD) as follows:

$$V = \left(LD\ \ x\ \ SD^2\right)\ \ x\ \ \frac{\pi}{6}$$

Additionally, cytotoxicity of MTS was determined using CCK-8 kit (Dojindo Laboratories, Kumamoto, Japan) and measured using 800™ TS Absorbance Reader (BioTek) as previously described.

2.7. Cell cycle analysis

Cell lines were seeded in 6-well plates at a density of 7×10^4 cells/well for LL/2 and 9×10^4 cells/well for A549. The next day, the medium was discarded and replaced for serum-free DMEM to synchronize cell cycle. After 24 h, the medium was replaced again for supplemented DMEM and treatments. LL/2 and A549 cell lines were treated with 16 μM and 1.6 μM of Bengamide II, respectively, which correspond to 4IC50 at 72 h during different times (12, 24 and 48 h). After treatment, medium was collected, and cells were harvested and centrifuged at 1500 g for 3 min. Pellet was resuspended in 100 μl of PBS and cells were fixed by adding 900 μl of 70% cold EtOH and placed on ice for 10 min. After that, cells were washed twice with PBS and DNA extraction solution (Na_2HPO_4 0.2 M diluted in 0.1 M acetic acid, pH 7.8) was added and incubated for 10 min at room temperature. DNA extraction solution was removed by centrifugation (300 g, 3 min) and pellets were incubated using the propidium iodide (PI)/RNASE solution (ImmunoStep) at 37 °C for 15 min in the dark. Subsequently cells were washed, and the results were obtained in BD FACSCanto II flow cytometer (BD BioSciences).

2.8. Western blot analysis

Proteins for western blot analysis were obtained from LL/2 and A549 cell lines treated with 4IC50 of Bengamide II (16 μM and 1.6 μM, respectively) at different time points (12, 24 and 48 h) and an untreated control was included. Cells were harvested and lysed with RIPA lysis & extraction buffer (G-Biosciences). Protein concentrations were determined using Bradford Reagent (Sigma-Aldrich) and then denatured in sodium dodecyl sulfate (SDS) loading buffer at 95ºC for 5 min. Equal amounts of total protein (60 μg) were separated by 12% SDS-polyacrylamide electrophoresis gels (SDS-PAGE) and then transferred onto nitrocellulose membranes (pore size 0.45 μm, Bio-Rad), blocked with 5% fat-free dry milk in 1X TBS (Thermo Fisher Scientific) containing 0.1% Tween 20 (Bio-Rad) at room temperature for 1 h. The primary antibodies were incubated overnight at 4ºC, followed immunoblotting with horseradish peroxidase-coupled secondary antibody for 1 h at room temperature. Finally, the bands corresponding to interest proteins were visualized using Amersham™ ECL™ Prime (Thermo Fisher Scientific) in the LAS-4000 mini equipment (GEHealthcare, Chicago, Illinois, EEU) and optical density (OD) values were quantified using Quantity One analytical software (Bio-Rad). Western Blot conditions and antibodies are shown in Table 1.

2.9. TUNEL staining

Apoptotic cell death in A549 and LL2 cell lines, control and treated with Bengamide II, was evaluated with terminal deoxynucleotidyl transferase-mediated dUTP nick end-labeling (TUNEL) staining using a TMR red *in situ* cell death detection kit (Roche). Cells were seeded at a density of 2×10^3 and 3×10^3 cells/well for LL2 and A549, respectively, in culture slides chambers (Corning Incorporated) and treated with four times the IC_{50} of Bengamide II (16 μM and 1.6 μM respectively) at different time points (12, 24 and 48 h) and an untreated control was included. After treatment, cells were fixed with 4% PFA at room temperature for 1 h. In addition, deparaffinized and rehydrated sections of tumor from mice were also analyzed by TUNEL analysis. Both, cells and tissue section were permeabilized with 0.1% Triton X-

Table 1
Western Blot conditions and antibodies.

Target	Supplier	Catalog no.	Working conditions (Dilution, Temperature and Time)
Primary antibodies			
Caspase-3	Invitrogen	700182	1:500, 4ºC, Overnight
VEGFA	Abcam	ab46154	1:1000, 4ºC, Overnight
LC3B	Novus Biologicals	NB100–2220	1:1000, 4ºC, Overnight
γ-H2AX	Invitrogen	MA1–2022	1:1000, 4ºC, Overnight
β-actin	Sigma-Aldrich	A3854	1:25000, Room Temperature, 1 h
Secondary antibodies			
Mouse IgG	Santa Cruz Biotech	sc-516102	1:5000, Room Temperature, 1 h
Rabbit IgG	Santa Cruz Biotech	sc-2357	1:5000, Room Temperature, 1 h

100 and 0.1% sodium citrate for 2 and 8 min, respectively, and then incubated with TUNEL reaction mixture at 37ºC in darkness for 60 min. After incubation, washes and staining with Hoechst (1:1000) for 5 min were performed. Apoptotic cells were observed by fluorescence microscopy (Leica). Finally, the number of TUNEL-positive cells in each of the conditions compared to the control was determined. Using ImageJ software, the TUNEL labeling intensity of each cell was quantified and, based on a threshold set from the control, positive and negative cells were counted.

2.10. Ki67 immunofluorescence

Immunofluorescence was performed to determine Ki67 expression. LL2 and A549 cell lines were seeded at a density of 2×10^3 and 3×10^3 cells/well, respectively, in culture slides chambers (Corning Incorporated) and treated with 4IC50 of Bengamide II (16 μM and 1.6 μM, respectively) at different time points (12, 24 and 48 h) and an untreated control was included. Cells were fixed with 95% cold methanol for 25 min at − 20ºC, permeabilized with 0.3% Triton X-100 diluted in 0.1% PBS-Tween for 10 min and blocked with 5% goat serum in 0.1% PBS-Tween for 30 min. After that, cells were incubated with primary anti-Ki67 antibody (BD, 550906, 1:50) for 1 h at room temperature and goat anti mouse IgG-FITC secondary antibody (SantaCruz Biotechnology, sc-2010, 1:100) for 1 h. Finally, nuclei staining was performed using Hoescht (1:1000). To analyze Ki67 expression in tumor from mice, samples were included in paraffin blocks and then cut with a rotary microtome (Leica). Sections were deparaffinized, hydrated and antigenic recovery was performed by incubating them in a heat vaporizer with 20% citrate buffer for 20 min. After cooling samples in distilled water, Ki67 staining was performed as previously and observed by fluorescence microscopy (Leica). For quantification of Ki67 labelling, the number of Ki67 foci in each cell nucleus was counted using ImageJ software.

2.11. Lysosomes staining

A549 and LL2 cell lines were seeded in 96-well plates and left overnight to attach and were treated with 4IC50 of Bengamide II (16 μM and 1.6 μM, respectively) at different time points (12, 24 and 48 h) and an untreated control was included. After treatment, lysosomal vesicles were stained with LysoTracker™ Red DND-99 (ThermoFisher Scientific) diluted to 50 nM concentration for 1 h, after which nucleus were stained with Hoechst (1:1000). The images were taken on live cells in PBS using a fluorescence microscopy (Leica). Quantification of the images was performed by analyzing the fluorescence intensity with ImageJ software.

2.12. In vivo assay

Immunocompetent female C57BL/6 mice (weight 18–22 g) (Charles River Laboratories Inc) were used to perform *in vivo* studies. Mice were housed in cages under controlled conditions (22 ± 2ºC and 12 light-dark cycle) and free access to water and food. The *in vivo* experiment was approved by the Research Ethics Committee of Granada University (Reference code: 16/01/2020/005) and in accordance with international standards (European Communities Council Directive 2010/63).

2.12.1. In vivo toxicity test

Fifteen mice were divided into three groups. The control group received saline solution and another two groups were treated with different doses of Bengamide II (10 and 20 mg/kg) intraperitoneally every two days for a total of 9 doses. Toxicity was monitored by recording body weights and deaths in each treatment cycle and by observation of general health. At the end point of the toxicity test, mice were sacrificed by isoflurane (Fatro) inhalation and extraction of complete peripheral blood from the mouse *via* axillary vessels was performed. To evaluate the possible impact of treatment in hematological parameters, mice blood was processed in Mslab21 Medical Lab Fully Auto Hematology Analyzer/Cbc Test Machine (Medsinglong Global Group Co, China) and hemograms were obtained.

2.12.2. In vivo tumoral induction

Subcutaneous and metastatic tumor models were induced and additionally, a group of healthy control mice were included in both assays. Subcutaneous tumors were induced by injecting 5×10^5 cells of LL/2 cell line resuspended in 100 μl of saline serum into the right flank of the mice. When tumors were palpable, mice were divided into two groups, a subcutaneous control group (n = 10) and a subcutaneous treated group (n = 10). Treated group was injected intraperitoneally with a dose of 20 mg/kg Bengamide II and control group was injected with saline solution. Each group was treated every two days (three times a week) for a total of 9 doses. The weights (controlled with a balance), tumor dimensions (measured with a digital caliper) and death of both groups of mice were recorded throughout the time. Tumor volume was calculated as follows:

$$V = \left(a \quad x \quad b^2\right) \quad x \quad \frac{\pi}{6}$$

Where "a" is the largest diameter of the tumor, and "b" the largest diameter perpendicular to "a". Day 32 from the inoculation of tumor cells (day 21 from the start of treatment) mice were sacrificed by isoflurane (Fatro) inhalation and extraction of complete peripheral blood from the mouse *via* axillary vessels was carried out. Tumors were excised, photographed and weighed. Finally, samples of tumors were fixed in paraformaldehyde 4% (PanReac) for further inclusion in paraffin. Additionally, tumor fragments were preserved in RNAlater (Sigma-Aldrich) at − 80ºC for further analysis.

Metastatic model was induced by injecting intravenously 1×10^6 of LL/2 cells resuspended in 100 μl of DMEM in the tail vein. Three days later, mice were divided into two groups, a metastatic control group (n = 9) and a metastatic treated group (n = 8). The treated group was injected intraperitoneally with a dose of 20 mg/kg Bengamide II and the control group was injected with saline solution. Each group was treated every two days (three times a week) for a total of 9 doses. Mice weights and deaths of both groups were recorded throughout the time. The endpoint of the experiment was on the day 34 from the inoculation of tumor cells (day 31 from the start of treatment). Mice were sacrificed by isoflurane (Fatro) inhalation and extraction of complete peripheral blood from the mouse *via* axillary vessels was done. In this case, the thoracic content was excised and lungs were filled with Bouin's solution (Sigma-Aldrich) during 24 h. After that, thoracic content was photographed, heart was removed, and lungs were weighed and then, lungs were embedded in paraffin.

2.13. Evaluation of organ damage

To collect serum, blood mice was kept for 15 min at room temperature and then centrifuged at 2000 g for 10 min. Serum was preserved at − 80ºC for further analysis. Organ damage was evaluated using reagent kits supplied by Spinreact (Girona, Spain) and following the manufacturer's instructions. The serum determinations performed were lactate dehydrogenase (LDH, Ref. 1001260), creatine (Ref. 1001110), amylase (Ref. 41201), total protein (Ref. 1001290), creatinine kinase MB isoenzyme (CK-MB, Ref. 1001054), creatinine kinase-NAC (CK-NAC, Ref. 41250), glutamate oxaloacetate (GOT, Ref. 1001160) and glutamate pyruvate transaminase (GPT, Ref. 1001170).

2.14. Histological analysis

Tumors included in paraffin blocks were cut with a rotary microtome (Leica). Sections were deparaffinized, hydrated and stained with hematoxylin-eosin.

2.15. RNA isolation and real-time quantitative polymerase chain reaction (RT-qPCR)

Tumor tissue preserved in RNAlater (Sigma-Aldrich) was mechanically homogenized. Total RNA was extracted using RNeasy Mini Kit (Qiagen) according to the manufacturer's instructions and quantified using Nanodrop 2000 (Thermo Fisher). The synthesis of complementary DNA was done using Reverse Transcription System kit (Promega) and RT-qPCR was run on StepOnePlus™ Real-Time PCR System (Applied Biosystem) and performed using TB Green Premix Ex Taq II (Takara Bio) according to the manufacturer's instructions. The primers used in RT-qPCR are listed in Table S1. *B-2-microglobulin* was used as reference gene. Gene expression was analyzed using $2^{-\Delta\Delta Ct}$ method. After that, fold change compared to control mice was calculated and data represented.

2.16. Statistical analysis

Different statistical tests were used depending on the type of data analyzed. All statistical analyses and images were performed with Graphad Prism 9. Comparisons between two groups were analyzed with Student t-test. One-way ANOVA (univariate comparison) and two-way ANOVA (comparison of two variables) were used for the comparison between several samples and Tukey's post-hoc test was performed. Non-linear regression was performed for the cytotoxicity analysis and logIC50 was calculated. Kaplan-Meier method was used to evaluate mice survival and log-rank test was performed. Differences with *p-value* < 0.05 were considered statistically significant.

3. Results and discussion

3.1. Synthesis of the Bengamide analogues

As mentioned above, we reported an alternative synthesis of bengamide analogue **8** according to the synthetic strategy delineated in our laboratories for the bengamides. However, in order to have access to sufficient amounts of analogue **8** for the *in vivo* studies, we considered that the cross-metathesis reaction should be carried out in earlier stages of the synthesis, prior to the peptidic coupling. According to this modification in the order of the synthetic steps, terminal olefin **9** was reacted with olefin **10** in the presence of Hoveyda-Grubbs 2nd generation catalyst to provide *E*-alkene **11** in an excellent 90% yield. Having been efficiently installed the olefin substituent, selective oxidation of the resulting disubstituted alkene **11** with TEMPO/BAIB furnished acid **12**, which, without further purification, was coupled with the amino acid derivative **13** by the action of the coupling reagent BOP to obtain the protected bengamide analogue **14** in 82% yield over 2 steps. Final acetal deprotection of **14** provided analogue **8** in an 83% yield. After that, NMR data (Fig. S1) confirmed that it was the Bengamide II molecule. This improved synthesis (Scheme 2) allowed us to have access to more than 100 mg for all the biological evaluations described herein.

3.2. Bengamide II reduces viability in a broad panel of cell lines

Cytotoxic effects of Bengamide II were evaluated in a panel of 21 tumoral and non-tumoral cell lines of different origin (breast, pancreas, lung, central nervous system, colon and liver) after 72 h of drug exposure. For each cell line, IC_{50} was calculated (Table 2).

IC_{50} values varied over a wide range from 0.16 to > 75 μM. The most pronounced effect on cell viability was observed in the lung cancer lines NCIH460 and A549 with IC_{50} values of 0.16 and 0.41 μM, respectively. This is in agreement with results obtained by other authors for other bengamides with antiproliferative effect against breast cancer cell lines MDA-MD-435 [22] and MCF7 [6], NSCLC and SCLC cell lines A549 and H1299 [9], colon cancer cell lines T84, SW480, HCT15, HT29 and MC38 [6] and other cancer cell types in the NCI60 cell-line panel [22] with IC_{50} values of nM-μM range. Furthermore, the non-tumor cell line MCF10A included in the *in vitro* assay showed IC_{50} value (1.82 μM) similar to the tumor cell lines. However, the colon non-tumor cell line, CCD18Co showed an IC_{50} > 75 μM. Among the murine tumor cell lines, the one from pancreas (Panc2) together with the one of pulmonary origin (LL2) showed a large reduction in viability with IC_{50} values of 1.09 μM and 4.02 μM, respectively, compared to the cell lines from breast, E0771 (IC_{50} = 19.54 μM) and colon, MC38 (IC_{50} = 28.88 μM). Taking together, low IC_{50} of Bengamide II in human lung cancer cell lines and in LL2 murine lung cancer cell line, this tumor type was selected for further *in vitro* studies and *in vivo* assay in immunocompetent mice.

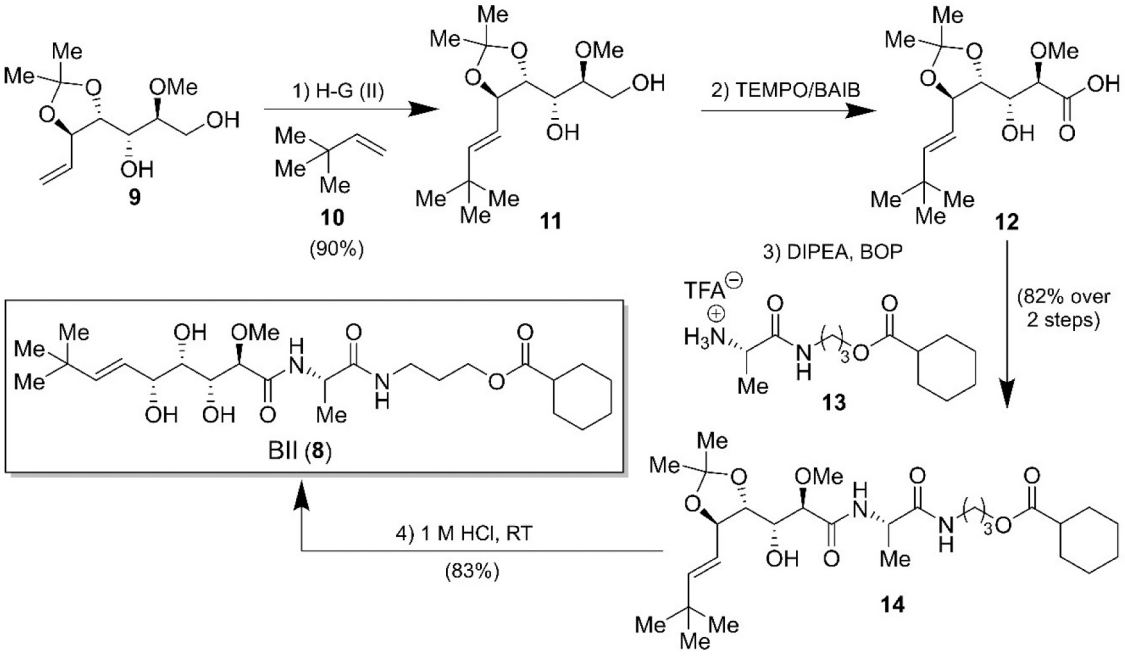

Scheme 2. An Improved Synthesis for Bengamide Analogue **8** (BII).

Table 2
Determination of $IC_{50}^{(a)}$ (μM) of Bengamide II in different cell lines.

Organ/Tissue	Cell line	Bengamide II IC_{50} (μM)
Breast	MCF7	0.50 ± 0.15
	MDA-MB-231	5.00 ± 0.07
	SKBR3	25.92 ± 8
	MCF10A	1.82 ± 0.31
	E0771	19.54 ± 1.27
Pancreas	Panc1	4.04 ± 0.61
	Panc2	1.09 ± 0.19
Lung	A549	0.41 ± 0.2
	NCI-H460	0.16 ± 0.02
	NCI-H520	> 75
	H69	4.80 ± 1.52
	LL2	4.02 ± 0.72
Central Nervous System	SK-N-SH	8.97 ± 1.02
	A172	1.11 ± 0.23
	SF268	29.52 ± 1.93
	LN229	1.35 ± 0.46
Colon	T84	1.35 ± 0.28
	CCD18Co	> 75
	MC38	28.88 ± 4.14
Liver	HepG2	14.98 ± 0.58

[(a)]Half-maximal inhibitory concentration (IC_{50}) values calculated from dose-response curves as the concentration of compound that inhibits cell survival by 50% compared to control. They are expressed as means ± SD of triplicate samples each.

3.3. Bengamide II reduces the colony-forming capacity of lung tumor cell lines

As shown in Fig. 1, all three lung cell lines treated with Bengamide II IC_{10} and IC_{25} at 72 h displayed a decreased capacity to form colonies in long-term experiment when seeded at low cell density. Concretely, the exposure of A549 (Fig. 1A), NCIH460 (Fig. 1B) and LL2 (Fig. 1C) to Bengamide II IC_{25} (0.1, 0.1 and 3 μM, respectively) showed an almost total reduction in colony forming capacity. In addition, the fraction of cells resistant to Bengamide II IC_{50} exposure for 72 h showed a slight reduction in colony forming ability that was not statistically significant in any of the cell lines tested.

3.4. Bengamide II inhibits growth of Multicellular Tumor Spheroid (MTS) from lung tumor cell lines

MTS were used to study the effects and penetrability of Bengamide II in a three-dimensional system that mimics 3D tumors *in vivo*. As shown in Fig. 1, cell viability at the end point of the experiment (9 days) measured by CCK8 showed a marked reduction in cell viability in all cell lines studied. Furthermore, a significant reduction in MTS size was also demonstrated after exposure to Bengamide II treatments (IC50, 2IC50, and 4IC50) indicating a dose-dependent response. Specifically, NCIH460 MTS treated with IC50, 2IC50, and 4IC50 of Bengamide II showed a 15.7%, 26% and 36.6% of size reduction respectively (Fig. 1**E**). LL2 MTS showed the most marked size differences with a reduction of 49.2%, 65.6% and 80.2% after the use of IC50, 2IC50, and 4IC50 of Bengamide II, respectively (Fig. 1**F**). Finally, only the A549 cell line did not show MTS volume differences despite a positive modulation of cell viability. However, MTS from A549 (Fig. 1**D**), NCIH460 (Fig. 1**E**) and LL2 (Fig. 1**F**) cell lines showed a dose-dependent reduction in viability on the endpoint of the experiment (Day 9).

The findings obtained in this MTS assay using Bengamide II demonstrated their potent antitumor effects within this three-dimensional arrangement, which more closely resembles an *in vivo* model due to the presence of chemical gradients (such as oxygen, nutrients, catabolites, or drugs) and the formation of a necrotic zone within the spheroids [23].

3.5. Modulation of cell cycle by Bengamide II

Morphological alterations were observed in A549 and LL2 cell lines subsequent to exposure to Bengamide II. Fig. 2A demonstrates that the A549 cell line exhibited a transition towards a more spherical morphology, while the LL2 cell line (Fig. 2B) displayed an elongated morphology following treatment with Bengamide II, in contrast to their corresponding control conditions.

A549 and LL2 cells lines treated with Bengamide II showed statistically significant changes in cell cycle analysis. A549 cell line showed a statistically significant ($p < 0.001$) G0/G1 phase increase with Bengamide II treatment at all treatment times. At longer times (24 and 48 h) a G2/M phase arrest was also observed (Fig. 2C). In LL2 cell line (Fig. 2D) an arrest in the G0/G1 phase of the cell cycle was observed at 12 and 24 h and basal levels were restored at 48 h. A G2/M arrest is also observed at 12 and 48 h of Bengamide II treatment. Furthermore, a significant reduction in the proportion of cells in the S phase of the cell cycle was observed in both A549 and LL2 cell lines. However, no changes in the SubG1 phase were observed in either cell line (Figs. 2E and F). The induction of cell cycle arrest in the G2/M phase by Bengamide II was similarly observed in a study conducted by Garcia Pinel et al. using the colon cancer cell line T84 [6]. Furthermore, Philips et al. revealed arrest in G1 and G2/M phases of cell cycle, data supported by western blot analysis of key cell cycle regulators [24].

3.6. Molecular mechanisms of Bengamide II treatment

In order to determine the molecular mechanism of cell death induced by Bengamide II, proteins involved in apoptosis mechanisms such as caspase 3 or autophagy such as LC3B were studied in A549 human non-small lung cancer cell line (Fig. 3A) and LL2 murine lung cancer cell line (Fig. 3B). Activation of caspase 3 was observed in A549 cell line and an increase of caspase-3 cleavage only after longer treatment times (48 h). Caspases maintain cellular homeostasis by modulating processes related to cell death and inflammation. They achieve this regulation through targeted proteolytic cleavage at specific aspartate residues within their substrate proteins, thus exerting precise control over cellular responses. Caspase-3 is an effector apoptotic caspase which has been associated with the treatment of different drugs used in the clinic for NSCLC, such as paclitaxel or cisplatin [25,26].

Western blot detection of LC3B derivates (LC3-I and LC3-II) revealed a time-dependent increase in LC3-II levels in A549, indicating autophagy process activation. An increase in LC3-II expression was also observed in LL2 cell line upon Bengamide II treatment, but was not time-dependent. LC3 proteins are essential in autophagy involved in biogenesis and transportation of autophagosomes. LC3-I is conjugated to phosphatidylethanolamine to form lipidated LC3-II, which remains in autophagosomes until autophagosomal fusion with lysosomes. Some drugs have been shown to have antitumor activity through the promotion of autophagy, such as metformin [27] and rapamycin [28,29]. A study in NSCLC linked high levels of LC3B to better prognosis and reduced tumor aggressiveness [30]. Finally, lysosome formation was analyzed by LysoTracker staining of acidic vesicles (Figs. 4A and B). As shown in Fig. 4E, in A549 the fluorescence intensity per Lysotracker cell presented a 1.37, 1.98 and 3.09 fold increase compared to untreated cells at 12, 24 and 48 h of Bengamide II treatment, respectively. On the other hand, in LL2 the Lysotracker fluorescence intensity increased at 12 h of Bengamide II treatment and was maintained at 24 and 48 h. The results showed a higher presence of these vesicles in treated cells compared to control cells in both cell lines, which supports the results obtained in the western blot with LC3-II expression.

Another analysis performed was VEGFA expression, which showed a progressive time-dependent decrease in Bengamide II treatment in both cell lines (Figs. 3 A and B). In various cancer types, including NSCLC, the targeting of angiogenesis pathways has emerged as an important therapeutic approach. Angiogenesis plays a crucial role in the growth,

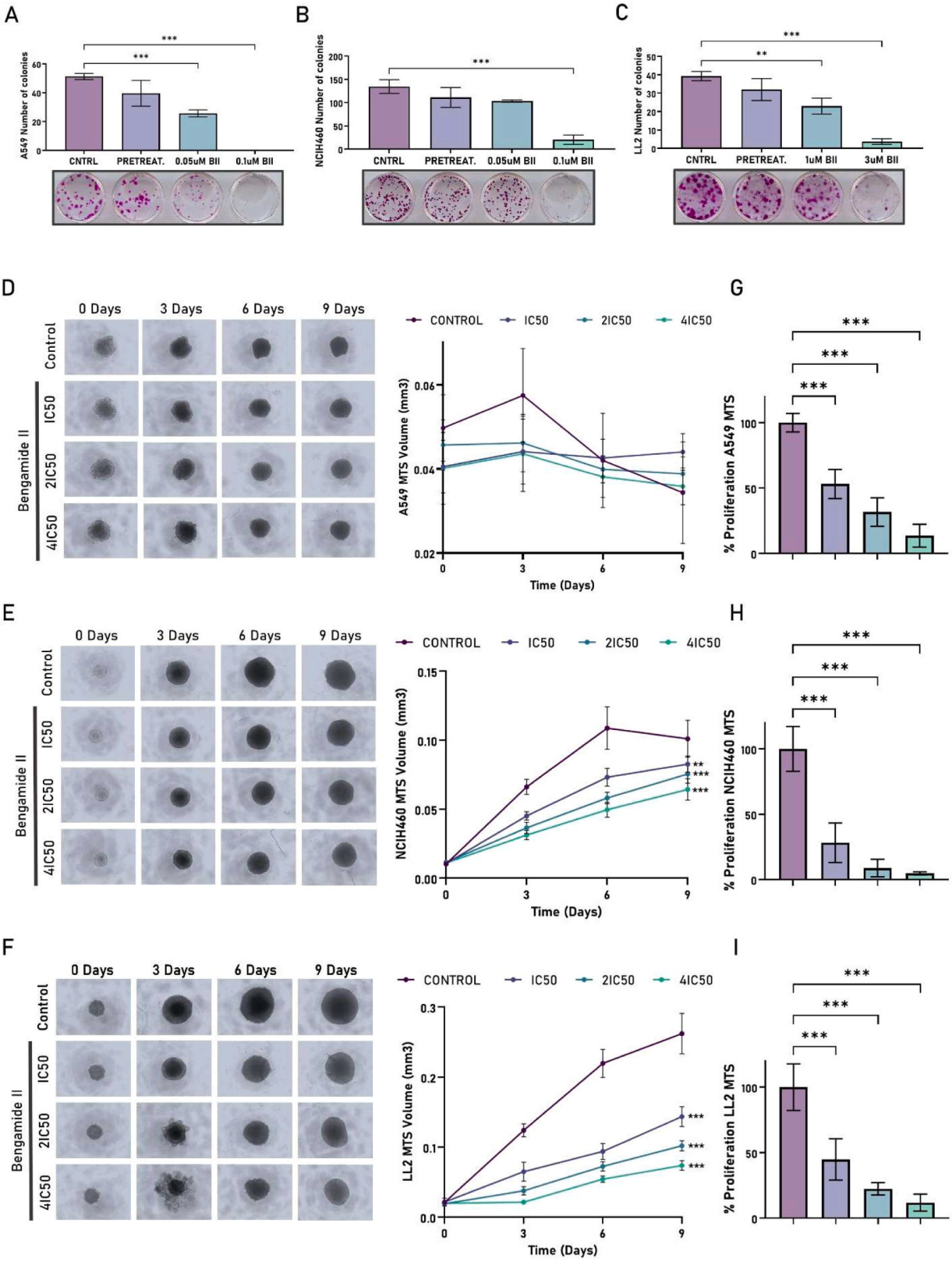

Fig. 1. Effect of Bengamide II on colony formation capacity and on growth modulation of Multicellular Tumor Spheroid (MTS). Colony growth analysis of A549 (A), NCIH460 (B) and LL2 (C) after IC50 Bengamide II (BII) pretreatment (72 h) (PRETREAT) and after IC10 (0.05, 0.05 and 1 μM respectively) and IC25 (0.1, 0.1 and 3 μM respectively) Bengamide II treatment. Data are presented as mean ± SD of three replicates *vs.* control. Representative images and graphic representation of A549 (D), NCIH460 (E) and LL2 (F) MTS volume (mm3) monitorization at different times after exposure to different doses of Bengamide II (IC50, 2IC50 and 4IC50). Untreated MTS were used as control. CCK8 analysis of A549 (G), NCIH460 (H) and LL2 (I) MTS at day 9. Data represent the mean value ± SD of 10 replicates. ** $p < 0.01$ and *** $p < 0.001$ *vs.* control.

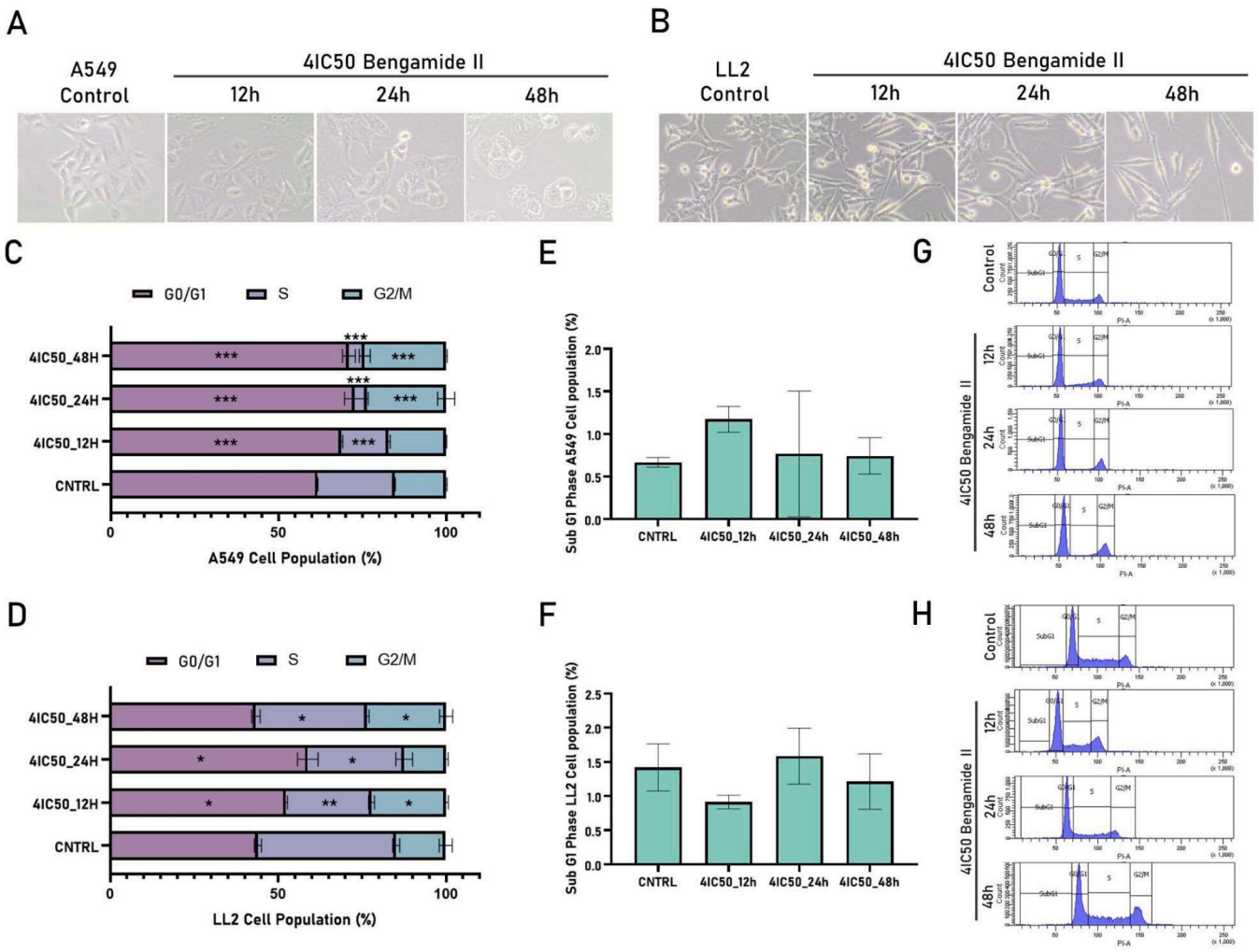

Fig. 2. Morphological changes and cell cycle modifications in lung cancer cell lines treated with Bengamide II. Cell morphology of A549 (A) and LL2 (B) cell lines in control cells and cells treated with Bengamide II. 40x Magnification. Graphical representation of G0/G1, S and G2/M phases of cell cycle analysis after treatment with 4IC50 of Bengamide II at different time points (12, 24 and 48 h) in A549 (C) and LL2 (D) cell lines. Modulation Sub G1 cell cycle phase by Bengamide II in A549 (E) and LL2 (F). Representative images of cell cycle analysis in A549 (G) and LL2 (H). Data represent the mean value ± SD of 3 replicates. * $p < 0.05$, ** $p < 0.01$ and *** $p < 0.001$ *vs.* control group.

proliferation, and metastasis of primary tumors. VEGF is the most important protein with proangiogenic functions. VEGF-A, specifically, acts as a potent inducer of angiogenesis and enhances vascular permeability by binding to its receptors. High levels of VEGF-A expression have been associated with poor prognosis [31] and reduced survival in lung adenocarcinoma [32].

DNA fragmentation plays a crucial role in inducing apoptosis and cell cycle arrest [33]. DNA double-strand breaks lead to phosphorylation of histone H2AX resulting in γ-H2AX. In LL2 cell line, a progressive increase in histone H2AX phosphorylation was observed with time of exposure to Bengamide II. In A549 the differences were less marked, with an increase in γ-H2AX expression at 12 and 48 h and matching the control at 24 h (Figs. 3 A and B). This indicates an increase in DNA double strand breaks after Bengamide II treatment. Furthermore, in this study, the TUNEL assay was employed to investigate the potential of Bengamide II in inducing apoptosis in tumor cells. Apoptotic cells undergo nuclear pyknosis characterized by condensed nuclei that break into fragments of varying sizes, leading to the formation of apoptotic bodies [34]. The results shown in Figs. 4A and B demonstrated minimal red fluorescence in the control cells of A549 and LL/2 following TUNEL staining. However, treatment of tumor cell lines with 4IC50 of Bengamide II revealed a significant presence of red fluorescence compared to the control group. Furthermore, an increase in the number of TUNEL-positive cells was found to be dependent on the duration of exposure to Bengamide II (Fig. 4C). In addition, the expression of the proliferation marker Ki67, implicated in tumor aggressiveness [35], was also studied. The number of Ki67 foci per cell were counted and represented in Fig. 4D. The analysis showed, in both cell lines, an increase in the number of cells without Ki67 labelling (n = 0 foci) and a reduction in the number of Ki67 foci per cell in a time-dependent manner.

3.7. *In vivo* toxicity assay

To determine the non-toxic Bengamide II dose in *in vivo* assay, a toxicity assay was performed using 10 and 20 mg Bengamide II/kg mouse (n = 5 per group). Our results showed that 10 and 20 mg Bengamide II/kg mouse treatment groups retained all individuals alive at the end of the experiment, with no apparent alterations in health status or body weight (Figs. 5A and B) and it did not induce any hematological abnormality (Table S2). Some of the systemic toxicities anticipated for bengamide B analogue, LAF389, in animal experimental studies included reversible myelosuppression, mainly lymphopenia [36]. However, our hematological analysis revealed no significant changes in lymphocyte levels, with the percentage of lymphocytes remaining stable and even exhibiting a slight increase following treatment with Bengamide II. Only a mild elevation in platelet counts was observed in the

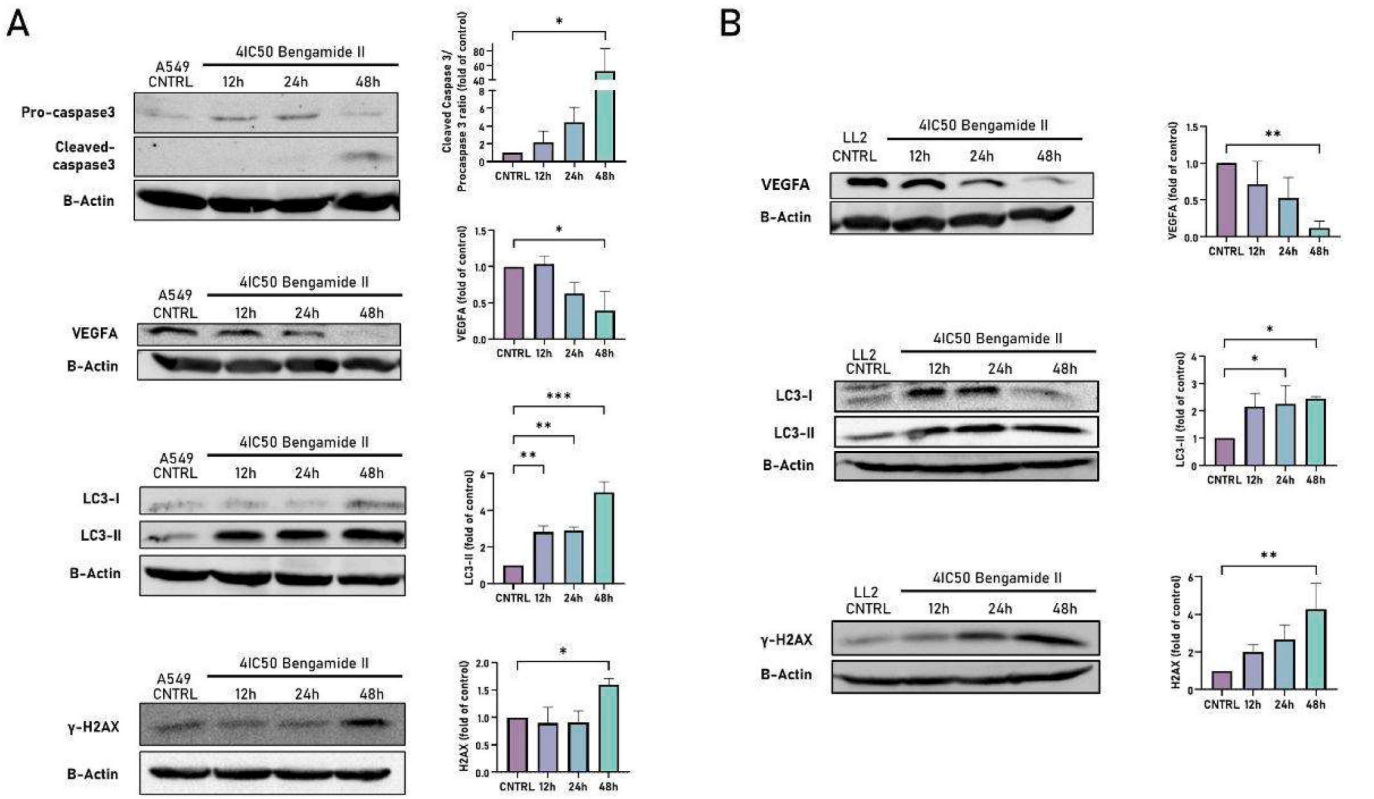

Fig. 3. Western Blot analysis of lung cancer cell lines treated with Bengamide II. Representative Western Blot and densitometric analysis of Caspase 3, VEGFA, LC3-II and γ-H2AX protein expression in A549 (A) and LL2 (B) lung cancer cell lines untreated (CNTRL) and treated with 4IC50 of Bengamide II at different time points (12, 24 and 48 h). β-actin was used as an internal control. Data represent the mean value ± SD of 3 replicates. * $p < 0.05$, ** $p < 0.01$ and *** $p < 0.001$ *vs.* control group.

Bengamide II-treated mice compared to the control group, yet these values fell within the normal range established for C57B/L female mice obtained from the commercial supplier Charles River.

Additionally, we assessed serum markers associated with cardiac, hepatic, renal, and pancreatic damage. Serum concentrations of cardiac muscle enzymes CK-MB, CK-NAC and LDH have been defined as biomarkers of heart diseases such as acute myocardial injury [37,38]. As shown in Fig. 5, after Bengamide II administration, serum concentrations of LDH (Fig. 5C and CK-NAC (Fig. 5D) remained unaltered, and CK-MB (Fig. 5E) showed a significant decrease at all doses of Bengamide II compared to control, indicating absence of cardiac damage. The elevation of serum amylase has been used as marker for pancreatic damage. The serum amylase level was measured, and results showed that there were no differences between healthy control mice and treated mice with Bengamide II at any dose (Fig. 5F). To estimate the toxicity of Bengamide II to liver, serum GPT and GOT were measured. Fig. 5G shows that serum GPT of Bengamide II treated mice was equal to those of healthy control mice, while serum GOT (Fig. 5H) was significantly decreased in treated mice compared to healthy control. Therefore, Bengamide II did not produce liver damage. As shown in Fig. 5I, creatinine levels in serum obtained after Bengamide II administration remained unaltered compared to healthy control group indicating no renal toxicity. Finally, total serum protein levels (Fig. 5J) did not show differences between groups.

Taken together, these findings demonstrate that Bengamide II did not induce any toxic side effects, and the myocardial, pancreatic, hepatic, and renal functions of the mice remained intact and functional. In contrast, a clinical trial conducted by Novartis involving the bengamide B analogue, LAF389 [39], in cancer patients (excluding leukemia) who were refractory to existing treatments, was prematurely discontinued due to the manifestation of cardiac toxicity signals, coupled with the absence of evident clinical activity [36]. Recent findings by García-Pinel et al. (2020) demonstrated the absence of toxic effects of bengamide analogues on blood cells and immune system cells, including macrophages and white blood cells [6]. Hence, the encouraging results regarding the favorable toxicity profile of our Bengamide II compound, which may exhibit enhanced suitability for clinical application, warrant continued advancement in *in vivo* studies involving tumor induction in immunocompetent mouse models.

3.8. *Bengamide II treatment significantly reduces subcutaneous tumor growth*

Subcutaneous induction of lung tumors in C57BL/6 with LL2 cell line was developed to determine the *in vivo* antitumor effect of Bengamide II. In terms of survival and mouse weight, no differences were observed between the control group and the treatment group with 20 mg/kg Bengamide II (Figs. 6A and 6B). As shown in Fig. 6C, the differences in tumor size were significantly evident in the last 3 measurement points, causing treatment with BII a reduction in tumor volume of 47% compared to the control group at the last point. At the end point of the experiment, these data were corroborated by weighing the excised tumors. Fig. 6D shows a 33.6% of tumor weight reduction in the treated group. Two additional *in vivo* studies have been conducted using bengamide analogues. In the study conducted by Kinder et al., the impact of a series of bengamide B analogues on tumor size reduction was assessed using the MDA-MB-435 xenograft model of human breast cancer. None of the analogues induced significant body weight loss or led to any mortality. Notably, the analogues tested at higher doses exhibited substantial tumor regression rates of 29% and 57% [40]. Wenzel et al. investigated the efficacy of a bengamide analogue in mice with early-stage subcutaneous B16 melanoma model. The authors administered a dose of 60 mg/kg, reaching a cumulative dose of 480 mg, which resulted in a 31% reduction in tumor size. However, it is important to

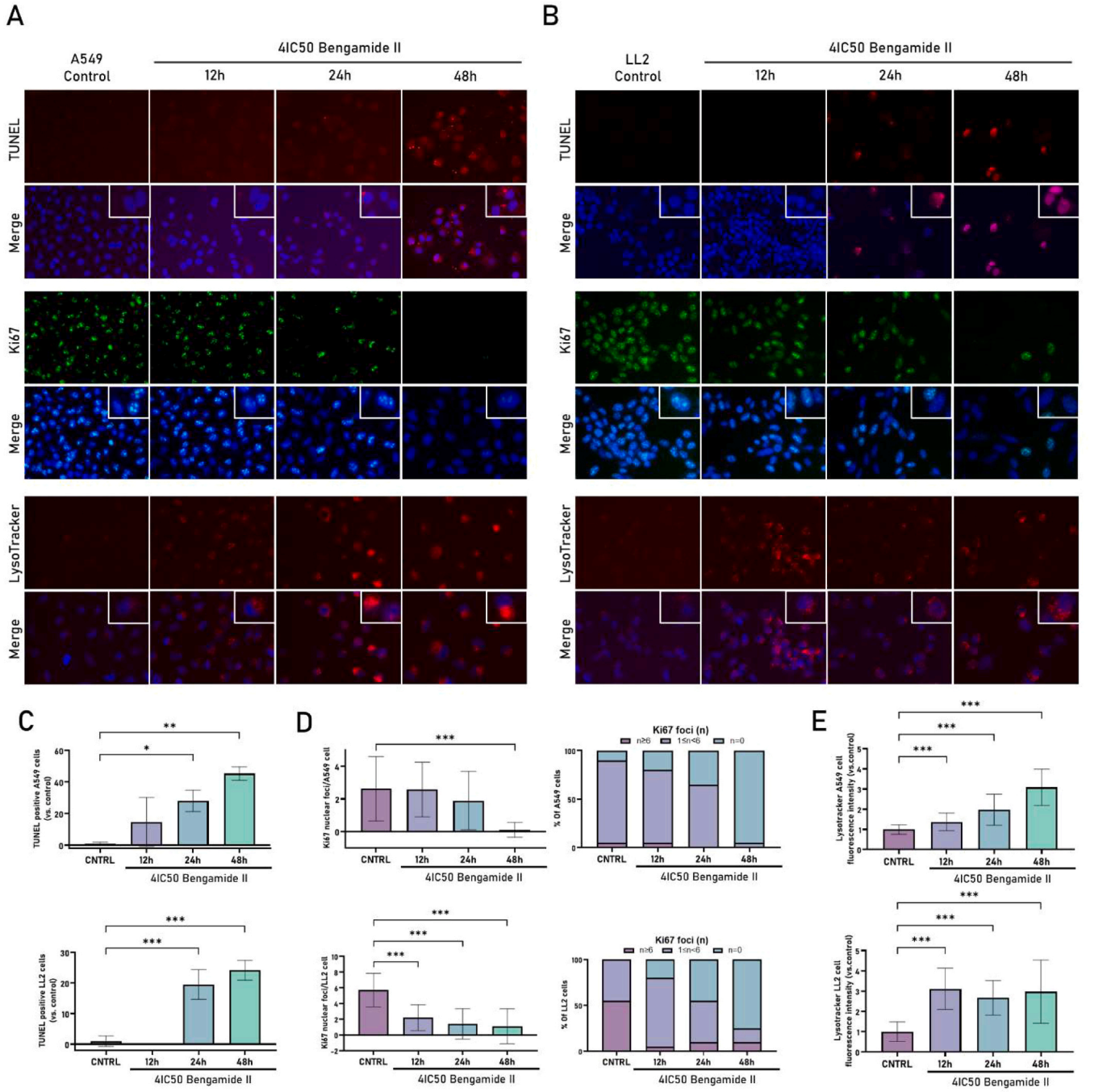

Fig. 4. Fluorescence microscopy analysis of lung cancer cell lines treated with Bengamide II. Representative fluorescence microscopy images of TUNEL assay, Ki67 proliferation marker and LysoTracker in A549 (A) and LL2 (B) cell lines. Nuclear staining was performed using Hoechst. Photos were taken using 40X magnification. Graphical TUNEL (C), Ki67 (D) and Lysotracker (E) fluorescence quantification. Data represent the mean value ± SD of 3 replicates. * $p < 0.05$, * * $p < 0.01$ and * ** $p < 0.001$ *vs.* control group.

note that the mice in the study exhibited a 14% decrease in body weight compared to the control group. Furthermore, two deaths were reported in the group of seven mice at a lower dose of the bengamide analogue (48.4 mg/kg) [13].

Interestingly, a RT-qPCR analysis of the tumor tissue of surviving mice showed a significant decrease in *EpCAM* expression after Bengamide II treatment (Fig. 6E). In NSCLC, elevated expression of *EpCAM* has been associated with unfavorable overall survival outcomes [41] and tumor progression [42]. *EpCAM* expression is also correlated with CD44 and CD166, and the presence of the triple-positive phenotype (EpCAM+/CD44 +/CD166 +) in NSCLC indicates higher self-renewal capacity, clonal heterogeneity, and gene expression associated with stemness [43]. Alibolandi et al. demonstrated that an aptamer-drug conjugate targeting EpCAM effectively inhibited the growth of lung cancer stem cells (CSCs) [44]. Therefore, given the effect of Bengamide II on EpCAM expression, this treatment could be advantageous and potentially contributing to a more favorable prognosis for lung cancer. Furthermore, the other markers analyzed by RT-qPCR did not show significant differences between the Bengamide II-treated group and control group, indicating that Bengamide II treatment did not select more aggressive or stem-like cancer cell populations nor those with increased proliferative capacity.

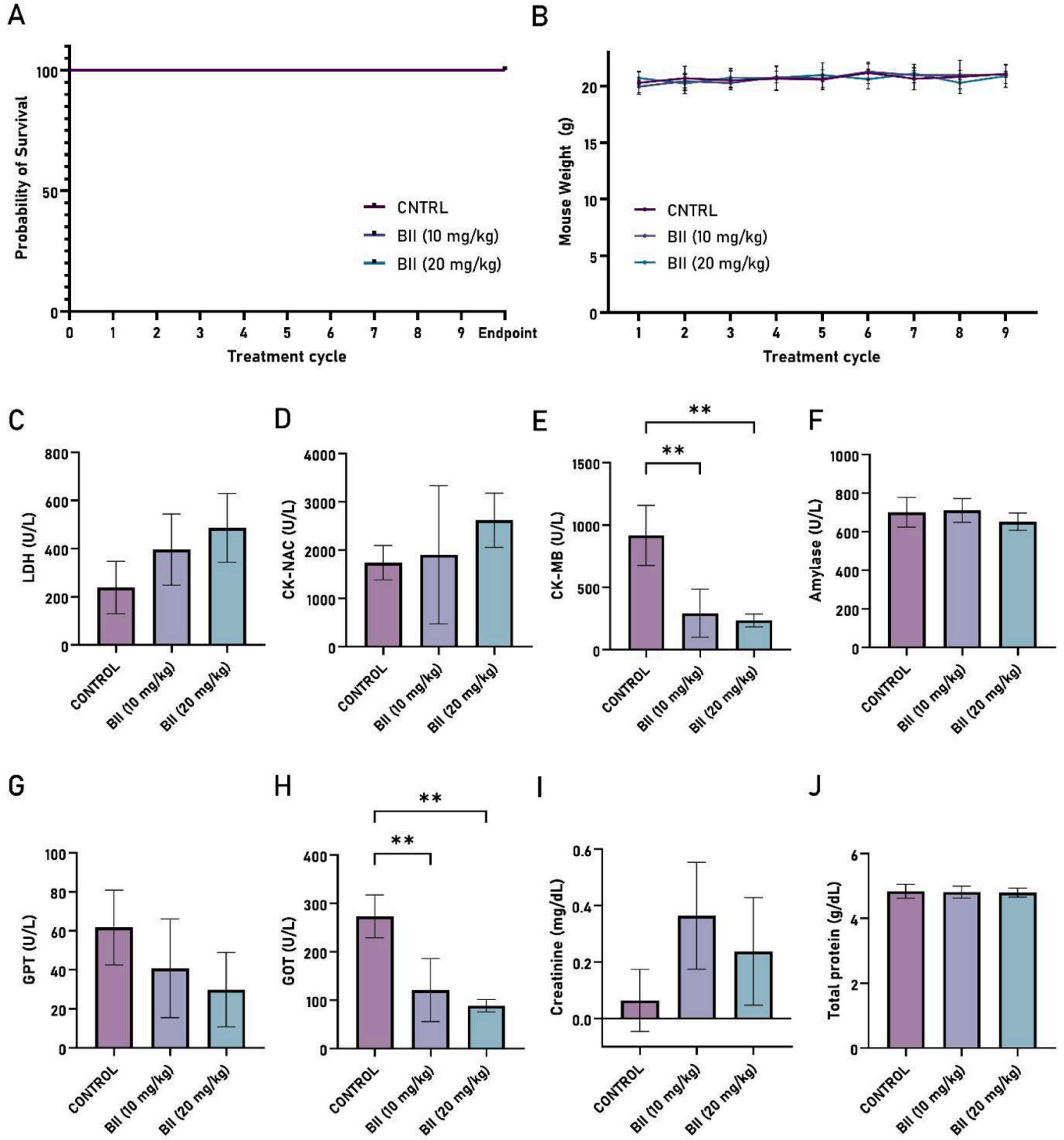

Fig. 5. *In vivo* toxicity assay. (A) Survival plot of different Bengamide II (BII)-treated mice groups. (B) Mouse weight monitorization among treatment cycles. Measurement of serum (C) lactate dehydrogenase (LDH), (D) creatinine kinase-NAC (CK-NAC), (E) creatinine kinase-MB (CK-MB), (F) amylase, (G) glutamate pyruvate transaminase (GPT), (H) glutamate oxaloacetate (GOT), (I) creatinine and (J) total protein. Data are represented as mean ± SD compared to each control. * $p < 0.05$, * * $p < 0.01$ and * ** $p < 0.001$.

The tumor damage in tumor-bearing mice, after Bengamide II treatment (20 mg/kg) was determined by Hematoxylin and Eosin (H&E) staining, TUNEL staining and Ki67 immunofluorescence assays (Fig. 6F). Histological evaluation by H&E suggested a slight reduction in vascularization after treatment with Bengamide II, although specific labeling of endothelial cells would be necessary to confirm this modulation. These preliminary results would be consistent with the reduction of VEGFA levels *in vitro* assays. In addition, compared to the control group, severe cell apoptosis occurred in the tumor tissues upon Bengamide II treatment compared to control group as indicated by TUNEL staining. The immunofluorescence images showed a higher labelling of the proliferation marker Ki67 in tumors of the control group compared to the Bengamide II treated group.

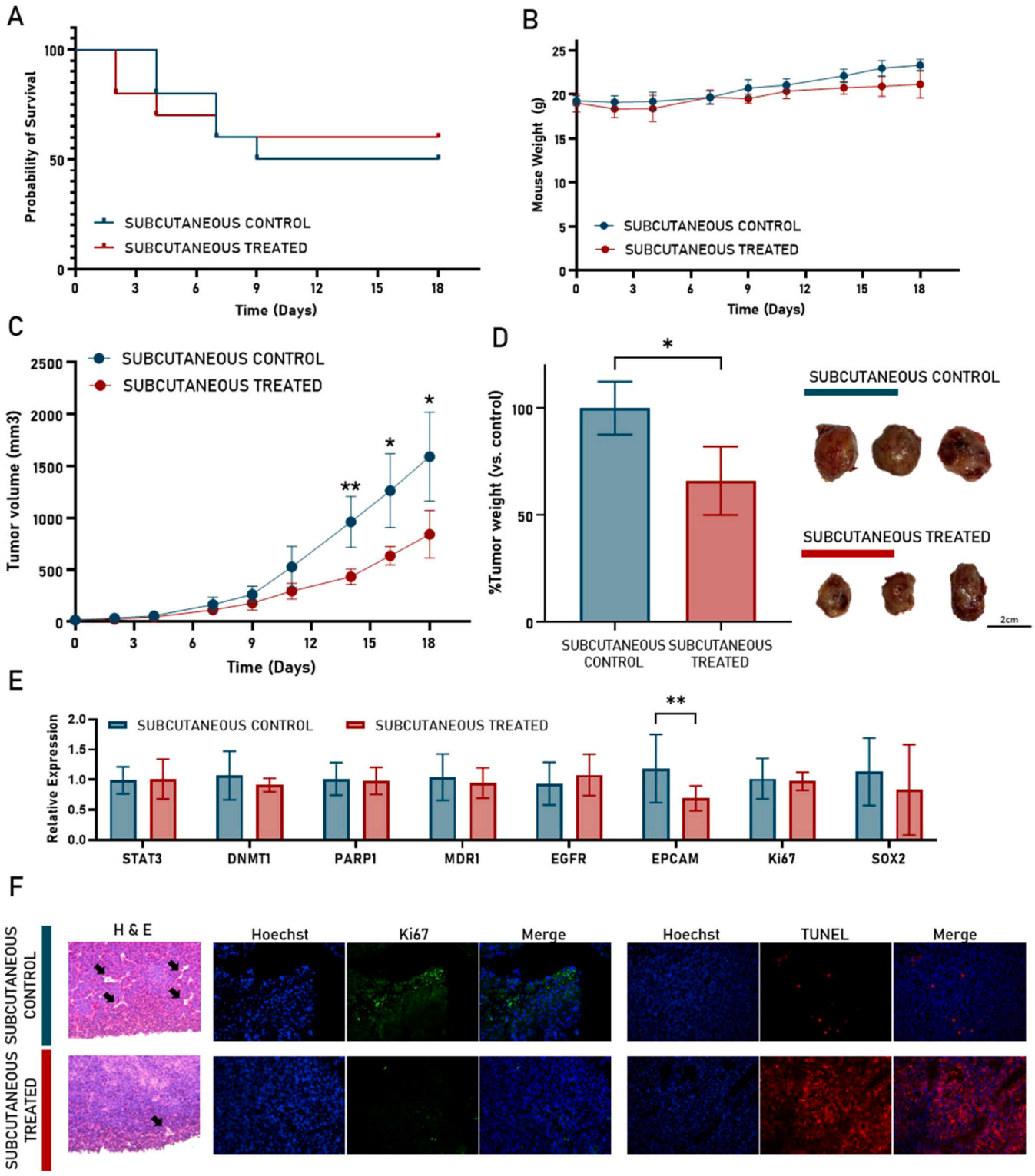

Fig. 6. *In vivo* subcutaneous tumor induction and follow up after treatment with Bengamide II. (A) Survival plot of mice after 9 Bengamide II treatment cycles. (B) Graphical representation of mice weights measured in each treatment cycle. Measurements were taken every 3 days and monitored for 18 days. (C) Representative images of subcutaneous tumor volume growth in C57BL/6 mice generated from the LL2 cell line. Untreated mice were used as controls. (D) Illustrative images of subcutaneous tumor size and representation of subcutaneous tumor weight (%) in C57BL/6 mice at the end point of the experiment. (E) RT-qPCR analysis of *STAT3*, *DNMT1*, *PARP1*, *MDR1*, *EGFR*, *EPCAM*, *KI67* and *SOX2* gene expression in tumors from subcutaneous control and treated mice groups. (F) Representative photographs of tumor sections derived from LL2 cell line with and without Bengamide II treatment, showing H&E staining, Ki67-positive cells (green) and TUNEL-positive cells (red). Sections were counterstained with Hoechst (blue). Photographs were taken at 20X magnification. Black arrows indicate areas of vascularization. Data represent the mean value ± SD. * $p < 0.05$, ** $p < 0.01$ and *** $p < 0.001$ *vs.* control group.

3.9. Bengamide II treatment significantly inhibited the formation of metastases from LL2

To determine the potential impact of Bengamide II on a model of cancer metastasis to lung, LL2 cells were injected into the tail vein of C57BL/6 mice. Interestingly, the Bengamide II treated group resulted in a significantly higher survival than the metastatic control group (non treated) (*p-value* = 0.019) (Fig. 7A). No differences in the weight of the mice were detected between both the metastatic control and the metastatic-treated groups (Fig. 7B). Metastases were assessed by gross morphology of the thoracic cavity (Fig. 7C) and % lung weight (Fig. 7D) at the end point of the experiment. Bengamide II treated mice showed few lung metastatic areas compared to metastatic control mice. H&E staining of lung sections and tissue examination showed substantially accelerated tumor growth with enhanced tumor burden and exhibited more tumor lesions in metastatic control group compared to mice treated with Bengamide II. Overall, the metastatic control group demonstrated a more evident and accelerated disease progression compared to the group of mice treated with Bengamide II. To date, there is limited knowledge regarding the impact of Bengamides on metastatic models. However, the preliminary findings indicated a substantial decrease in the size of metastatic regions (as determined by lung weight) and an improvement in overall survival rates in the treated group.

4. Conclusion

We have synthesized a new bengamide analogue, named Bengamide II, which showed a potent cytotoxic effect against a wide panel of tumor cell lines. We focused our assays on the antitumor activity of Bengamide II against lung cancer due to its poor prognosis and the need to develop new treatments. Bengamide II was able to inhibit cell viability in 2D (reducing the ability to form colonies) and 3D (reducing the growth of MTS) *in vitro* systems. In addition, cells treated with Bengamide II showed G2/M and G0/G1 cell cycle arrest, along with a decrease in the proliferation marker Ki67, associated with poor tumor prognosis. Regarding the mechanism of action, Bengamide II induced the production of acid vesicles and increased the autophagy through LC3-II signaling, with activation of caspase-3 and DNA fragmentation during the earliest stages of programmed cell death or apoptosis. In addition, Bengamide II showed a reduction in VEGFA, which may be involved in decreasing angiogenesis, a key process in tumor metastasis phenomena. *In vivo* studies showed that Bengamide II markedly reduced tumor volume and metastases, increasing survival. Interestingly, Bengamide II lacks systemic and hematological toxicities at the doses used with antitumor effect. In summary, the chemically synthesized bengamide analogue Bengamide II, is a promising drug for the lung cancer treatment showing relevant antitumor activity and significant safety. Although more research will be necessary to broaden our knowledge of this molecule, Bengamide II may be a new therapeutic tool for this type of tumor.

Funding

This research was funded by Junta de Andalucía through project

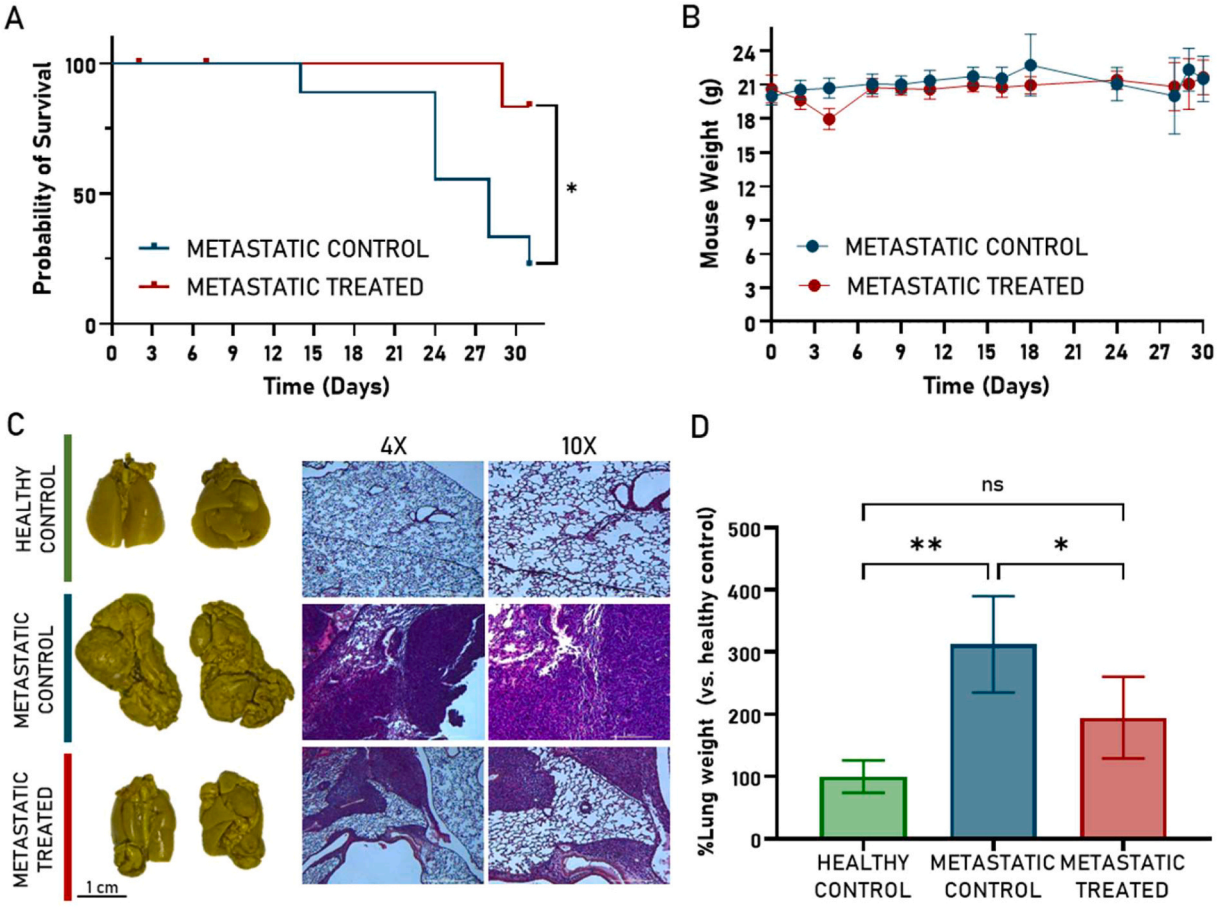

Fig. 7. *In vivo* metastatic model induction and follow up after treatment with Bengamide II. (A) Survival plot of mice after 9 Bengamide II treatment cycles. (B) Graphical representation of mice weights measured in each treatment cycle. Measurements were monitored for 30 days. (C) Illustrative images of thoracic cavity of C57BL/6 metastatic model mice generated from the LL2 cell line and Haematoxylin and Eosin staining. Untreated mice were used as controls. (D) Graphical representation of lung weight (%) in C57BL/6 mice at the experiment end point.

FP20_00540/FEDER and partially through the Projects A-CTS-666-UGR20 and RTI2018-098296-BI00 (MINECO and FEDER). In addition, this work was supported by research group CTS-107(Andalusian Government). A.O. acknowledges FPU2020 grant (ref. FPU20/07083) from the Ministerio de Educación y Formación Profesional (Spain).

CRediT authorship contribution statement

A. Ortigosa-Palomo: Investigation, Formal analysis, Writing – original draft. **C. Porras-Alcalá:** Investigation, Formal analysis. **F. J. Quiñonero:** Investigation, Formal analysis. **F. Moya-Utrera**: Investigation, Formal analysis. **R. Ortiz:** Conceptualization, Writing – original draft. **J. M. López-Romero:** Conceptualization, Writing – original draft. **C. Melguizo:** Conceptualization, Writing – original draft. **F. Sarabia:** Conceptualization, Writing – original draft. **J. Prados:** Conceptualization, Writing – original draft. All authors reviewed the manuscript and provided comments or suggestions. All authors read and approved the final manuscript.

Declaration of Competing Interest

The authors declare that they have no known competing financial interests or personal relationships that could have appeared to influence the work reported in this paper.

Acknowledgments

We thank Instrumentation Scientific Center (CIC) from University of Granada for technical assistance and the FQM397 research group of the University of Malaga.

Appendix A. Supporting information

Supplementary data associated with this article can be found in the online version at doi:10.1016/j.biopha.2023.115789.

References

[1] E. Quinoa, M. Adamczeski, P. Crews, G.J. Bakus, Bengamides, heterocyclic anthelmintics from a Jaspidae marine sponge, J. Org. Chem. 51 (1986) 4494–4497, https://doi.org/10.1021/jo00373a036.

[2] K.N. White, K. Tenney, P. Crews, The bengamides: a mini-review of natural sources, analogues, biological properties, biosynthetic origins, and future prospects, J. Nat. Prod. 80 (2017) 740–755, https://doi.org/10.1021/acs.jnatprod.6b00970.

[3] T.A. Johnson, J. Sohn, Y.M. Vaske, K.N. White, T.L. Cohen, H.C. Vervoort, K. Tenney, F.A. Valeriote, L.F. Bjeldanes, P. Crews, Myxobacteria versus sponge-derived alkaloids: the bengamide family identified as potent immune modulating agents by scrutiny of LC-MS/ELSD libraries, Bioorg. Med. Chem. 20 (2012) 4348–4355, https://doi.org/10.1016/j.bmc.2012.05.043.

[4] C. García-Ruiz, F. Sarabia, Chemistry and biology of bengamides and bengazoles, bioactive natural products from Jaspis sponges, Mar. Drugs 12 (2014) 1580–1622, https://doi.org/10.3390/md12031580.

[5] C. Porras-Alcalá, F. Moya-Utrera, M. García-Castro, A. Sánchez-Ruiz, J.M. López-Romero, M.S. Pino-González, A. Díaz-Morilla, S. Kitamura, D.W. Wolan, J. Prados, C. Melguizo, I. Cheng-Sánchez, F. Sarabia, The development of the bengamides as new antibiotics against drug-resistant bacteria, Mar. Drugs 20 (2022), https://doi.org/10.3390/md20060373.

[6] B. García-Pinel, C. Porras-Alcalá, L. Cabeza, R. Ortiz, J. Prados, C. Melguizo, I. Cheng-Sánchez, J.M. López-Romero, F. Sarabia, Bengamide analogues show a potent antitumor activity against colon cancer cells: a preliminary study, Mar. Drugs 18 (2020) 240, https://doi.org/10.3390/md18050240.

[7] H. Towbin, K.W. Bair, J.A. DeCaprio, M.J. Eck, S. Kim, F.R. Kinder, A. Morollo, D. R. Mueller, P. Schindler, H.K. Song, J. Van Oostrum, R.W. Versace, H. Voshol, J. Wood, S. Zabludoff, P.E. Phillips, Proteomics-based target identification: Bengamides as a new class of methionine aminopeptidase inhibitors, J. Biol. Chem. 278 (2003) 52964–52971, https://doi.org/10.1074/jbc.M309039200.

[8] W. Xu, J.P. Lu, Q.Z. Ye, Structural analysis of bengamide derivatives as inhibitors of methionine aminopeptidases, J. Med. Chem. 55 (2012) 8021–8027, https://doi.org/10.1021/jm3008695.

[9] S. Kim, K. LaMontagne, M. Sabio, S. Sharma, R.W. Versace, N. Yusuff, P.E. Phillips, Depletion of methionine aminopeptidase 2 does not alter cell response to fumagillin or bengamides, Cancer Res 64 (2004) 2984–2987, https://doi.org/10.1158/0008-5472.CAN-04-0019.

[10] X. Hu, Y. Dang, K. Tenney, P. Crews, C.W. Tsai, K.M. Sixt, P.A. Cole, J.O. Liu, Regulation of c-Src nonreceptor tyrosine kinase activity by bengamide a through inhibition of methionine aminopeptidases, Chem. Biol. 14 (2007) 764–774, https://doi.org/10.1016/j.chembiol.2007.05.010.

[11] E.C. Griffith, Z. Su, B.E. Turk, S. Chen, Y.H. Chang, Z. Wu, K. Biemann, J.O. Liu, Methionine aminopeptidase (type 2) is the common target for angiogenesis inhibitors AGM-1470 and ovalicin, Chem. Biol. 4 (1997) 461–471, https://doi.org/10.1016/S1074-5521(97)90198-8.

[12] N. Sin, L. Meng, M.Q.W. Wang, J.J. Wen, W.G. Bornmann, C.M. Crews, The anti-angiogenic agent fumagillin covalently binds and inhibits the methionine aminopeptidase, MetAP-2, Proc. Natl. Acad. Sci. U. S. A. 94 (1997) 6099–6103, https://doi.org/10.1073/pnas.94.12.6099.

[13] S.C. Wenzel, H. Hoffmann, J. Zhang, L. Debussche, S. Haag-Richter, M. Kurz, F. Nardi, P. Lukat, I. Kochems, H. Tietgen, D. Schummer, J.P. Nicolas, L. Calvet, V. Czepczor, P. Vrignaud, A. Mühlenweg, S. Pelzer, R. Müller, M. Brönstrup, Production of the bengamide class of marine natural products in myxobacteria: biosynthesis and structure-activity relationships, Angew. Chem. - Int. Ed. 54 (2015) 15560–15564, https://doi.org/10.1002/anie.201508277.

[14] W.-Y. Tai, R.-T. Zhang, Y.-M. Ma, M. Gu, G. Liu, J. Li, F.-J. Nan, Design, synthesis, and biological evaluation of ring-opened bengamide analogues, ChemMedChem 6 (2011) 1555–1558, https://doi.org/10.1002/cmdc.201100164.

[15] H. Sung, J. Ferlay, R.L. Siegel, M. Laversanne, I. Soerjomataram, A. Jemal, F. Bray, Global cancer statistics 2020: GLOBOCAN estimates of incidence and mortality worldwide for 36 cancers in 185 countries, Ca. Cancer J. Clin. 71 (2021) 209–249, https://doi.org/10.3322/caac.21660.

[16] A.A. Thai, B.J. Solomon, L.V. Sequist, J.F. Gainor, R.S. Heist, Lung cancer, Lancet 398 (2021) 535–554, https://doi.org/10.1016/S0140-6736(21)00312-3.

[17] N. Howlader, G. Forjaz, M.J. Mooradian, R. Meza, C.Y. Kong, K.A. Cronin, A. B. Mariotto, D.R. Lowy, E.J. Feuer, The effect of advances in lung-cancer treatment on population mortality, N. Engl. J. Med. 383 (2020) 640–649, https://doi.org/10.1056/nejmoa1916623.

[18] V.S. Iglesias, L. Giuranno, L.J. Dubois, J. Theys, M. Vooijs, Drug resistance in non-small cell lung cancer: a potential for NOTCH targeting? Front. Oncol. 8 (2018) https://doi.org/10.3389/fonc.2018.00267.

[19] S.B. Knight, P.A. Crosbie, H. Balata, J. Chudziak, T. Hussell, C. Dive, Progress and prospects of early detection in lung cancer, Open Biol. 7 (2017), https://doi.org/10.1098/rsob.170070.

[20] C. Hu, S. Meiners, C. Lukas, G.T. Stathopoulos, J. Chen, Role of exosomal microRNAs in lung cancer biology and clinical applications, Cell Prolif. 53 (2020), e12828, https://doi.org/10.1111/cpr.12828.

[21] K. Doello, C. Mesas, F. Quiñonero, G. Perazzoli, L. Cabeza, J. Prados, C. Melguizo, R. Ortiz, The antitumor activity of sodium selenite alone and in combination with gemcitabine in pancreatic cancer: an in vitro and in vivo study, Cancers (Basel) 13 (2021) 3169, https://doi.org/10.3390/cancers13133169.

[22] Z. Thale, F.R. Kinder, K.W. Bair, J. Bontempo, A.M. Czuchta, R.W. Versace, P. E. Phillips, M.L. Sanders, S. Wattanasin, P. Crews, Bengamides revisited: new structures and antitumor studies, J. Org. Chem. 66 (2001) 1733–1741, https://doi.org/10.1021/jo001380.

[23] M. Zanoni, F. Piccinini, C. Arienti, A. Zamagni, S. Santi, R. Polico, A. Bevilacqua, A. Tesei, 3D tumor spheroid models for in vitro therapeutic screening: A systematic approach to enhance the biological relevance of data obtained, Sci. Rep. 6 (2016), https://doi.org/10.1038/srep19103.

[24] P.E. Phillips, K.W. Bair, j. Bontempo, P. Crews, M. Czuchta, F.R. Kinder, R. W. Versace, B. Wang, J. Wang, A. Wood, S. Zabludoff, Bengamide E arrests cells at the G1/S restriction point and within the G2/M phase of the cell cycle, Proc. Am. Assoc. Cancer Res. 41 (2000) 59.

[25] C. cheng Zhang, C. guang Li, Y. feng Wang, L. hui Xu, X. hui He, Q. zhen Zeng, C. ying Zeng, F. yi Mai, B. Hu, D. yun Ouyang, Chemotherapeutic paclitaxel and cisplatin differentially induce pyroptosis in A549 lung cancer cells via caspase-3/GSDME activation, Apoptosis 24 (2019) 312–325, https://doi.org/10.1007/s10495-019-01515-1.

[26] T.L. Weigel, M.T. Lotze, P.K. Kim, A.A. Amoscato, J.D. Luketich, C. Odoux, Paclitaxel-induced apoptosis in non-small cell lung cancer cell lines is associated with increased caspase-3 activity, J. Thorac. Cardiovasc. Surg. 119 (2000) 795–803, https://doi.org/10.1016/S0022-5223(00)70016-X.

[27] M. De Santi, G. Baldelli, A. Diotallevi, L. Galluzzi, G.F. Schiavano, G. Brandi, Metformin prevents cell tumorigenesis through autophagy-related cell death, Sci. Rep. 9 (2019), 66, https://doi.org/10.1038/s41598-018-37247-6.

[28] X. Lin, L. Han, J. Weng, K. Wang, T. Chen, Rapamycin inhibits proliferation and induces autophagy in human neuroblastoma cells, Biosci. Rep. 38 (2018), https://doi.org/10.1042/BSR20181822.

[29] Y. Li, F. Liu, Y. Wang, D. Li, F. Guo, L. Xu, Z. Zeng, X. Zhong, K. Qian, Rapamycin-induced autophagy sensitizes A549 cells to radiation associated with DNA damage repair inhibition, Thorac. Cancer 7 (2016) 379–386, https://doi.org/10.1111/1759-7714.12332.

[30] A.M. Schläfli, O. Adams, J.A. Galván, M. Gugger, S. Savic, L. Bubendorf, R. A. Schmid, K.F. Becker, M.P. Tschan, R. Langer, S. Berezowska, Prognostic value of the autophagy markers LC3 and p62/SQSTM1 in early-stage non-small cell lung cancer, Oncotarget 7 (2016) 39544–39555, https://doi.org/10.18632/oncotarget.9647.

[31] S. Qin, M. Yi, D. Jiao, A. Li, K. Wu, Distinct roles of VEGFA and ANGPT2 in lung adenocarcinoma and squamous cell carcinoma, J. Cancer 11 (2020) 153–167, https://doi.org/10.7150/jca.34693.

[32] W.Y. Jung, K.W. Min, Y.H. Oh, Increased VEGF-A in solid type of lung adenocarcinoma reduces the patients' survival, Sci. Rep. 11 (1) (2021) 9, https://doi.org/10.1038/s41598-020-79907-6.

[33] J.Y.J. Wang, DNA damage and apoptosis, Cell Death Differ. 8 (2001) 1047–1048, https://doi.org/10.1038/sj.cdd.4400938.
[34] L.A. Burgoyne, The mechanisms of pyknosis: hypercondensation and death, Exp. Cell Res. 248 (1999) 214–222, https://doi.org/10.1006/excr.1999.4406.
[35] J. Xu, P. Liu, J. Da, J. Hao, W. Peng, G. Sun, Prognostic value of Ki-67 in stage I non-small-cell lung cancer: a meta-analysis involving 1931 patients, Pathol. Res. Pract. 215 (2019) 855–860, https://doi.org/10.1016/j.prp.2019.02.020.
[36] H. Dumez, H. Gall, R. Capdeville, C. Dutreix, A.T. Van Oosterom, G. Giaccone, A phase I and pharmacokinetic study of LAF389 administered to patients with advanced cancer, Anticancer. Drugs 18 (2007) 219–225, https://doi.org/10.1097/CAD.0b013e328010ef5b.
[37] S.Y. Kim, J.P. Lee, W.R. Shin, I.H. Oh, J.Y. Ahn, Y.H. Kim, Cardiac biomarkers and detection methods for myocardial infarction, Mol. Cell. Toxicol. 18 (2022) 443–455, https://doi.org/10.1007/s13273-022-00287-1.
[38] R. Klein, O. Nagy, C. Tóthová, F. Chovanová, Clinical and diagnostic significance of lactate dehydrogenase and its isoenzymes in animals, Vet. Med. Int. 2020 (2020), https://doi.org/10.1155/2020/5346483.
[39] D.D. Xu, O. Repič, T.J. Blacklock, L. Waykole, J.V. Calienni, L. Ciszewski, G.T. Lee, W. Liu, J. Szewczyk, K. Vargas, K. Prasad, An expedient synthesis of LAF389, a bengamide b analogue, Org. Process Res. Dev. 7 (2003) 856–865, https://doi.org/10.1021/op0341162.
[40] F.R. Kinder, R.W. Versace, K.W. Bair, J.M. Bontempo, D. Cesarz, S. Chen, P. Crews, A.M. Czuchta, C.T. Jagoe, Y. Mou, R. Nemzek, P.E. Phillips, L.D. Tran, R. Wang, S. Weltchek, S. Zabludoff, Synthesis and antitumor activity of ester-modified analogues of bengamide B, J. Med. Chem. 44 (2001) 3692–3699, https://doi.org/10.1021/jm010188c.
[41] N. Zhou, H. Wang, H. Liu, H. Xue, F. Lin, X. Meng, A. Liang, Z. Zhao, Y.J. Liu, H. Qian, MTA1-upregulated EpCAM is associated with metastatic behaviors and poor prognosis in lung cancer, J. Exp. Clin. Cancer Res. 34 (2015), https://doi.org/10.1186/s13046-015-0263-1.
[42] H.N. Chen, K.H. Liang, J.K. Lai, C.H. Lan, M.Y. Liao, S.H. Hung, Y.T. Chuang, K. C. Chen, W.W.F. Tsuei, H.C. Wu, EpCAM signaling promotes tumor progression and protein stability of PD-L1 through the EGFR pathway, Cancer Res 80 (2020) 5035–5050, https://doi.org/10.1158/0008-5472.CAN-20-1264.
[43] N.A. Satar, K.S. Fakiruddin, M.N. Lim, P.L. Mok, N. Zakaria, N.A. Fakharuzi, A. Z. Abd Rahman, Z. Zakaria, B.H. Yahaya, P. Baharuddin, Novel triple-positive markers identified in human non-small cell lung cancer cell line with chemotherapy-resistant and putative cancer stem cell characteristics, Oncol. Rep. 40 (2018) 669–681, https://doi.org/10.3892/or.2018.6461.
[44] M. Alibolandi, M. Ramezani, K. Abnous, F. Sadeghi, F. Atyabi, M. Asouri, A. A. Ahmadi, F. Hadizadeh, In vitro and in vivo evaluation of therapy targeting epithelial-cell adhesion-molecule aptamers for non-small cell lung cancer, J. Control. Release 209 (2015) 88–100, https://doi.org/10.1016/j.jconrel.2015.04.026.